MIT Libraries | DSpace@MIT

MIT Open Access Articles

Correlation chemical shift imaging with low-power adiabatic pulses and constant-density spiral trajectories

Massachusetts Institute of Technology

Correlation chemical shift imaging with low-power adiabatic pulses and constant-density spiral trajectories

Ovidiu C. Andronesi[1,#,*], **Borjan A. Gagoski**[2,#], **Elfar Adalsteinsson**[2,3], and **A. Gregory Sorensen**[1]

[1]Martinos Center for Biomedical Imaging, Department of Radiology, Massachusetts General Hospital, Harvard Medical School, Boston, MA 02114

[2]Department of Electrical Engineering and Computer Science, Massachusetts Institute of Technology, Cambridge, MA 02139

[3]Harvard-MIT Division of Health Sciences and Technology, Massachusetts Institute of Technology, Cambridge, MA 02139

Abstract

In this work we introduce the concept of correlation chemical shift imaging (CCSI). Novel CCSI pulse sequences are demonstrated on clinical scanners for two-dimensional COSY (Correlation Spectroscopy) and TOCSY (Total Correlation Spectroscopy) imaging experiments. To date there has been limited progress reported towards a feasible and robust multivoxel 2D COSY. Localized 2D TOCSY imaging is shown first time in this work. Excitation with adiabatic GOIA-W(16,4) pulses (Gradient Offset Independent Adiabaticity Wurst modulation) provides minimal chemical shift displacement error, reduced lipid contamination from subcutaneous fat, uniform optimal flip angles, and efficient mixing for coupled spins, while enabling short repetition times due to low power requirements. Constant-density spiral readout trajectories are used to acquire simultaneously two spatial dimensions and f_2 frequency dimension in (k_x, k_y, t_2) space in order to speed up data collection, while f_1 frequency dimension is encoded by consecutive time increments of t_1 in (k_x, k_y, t_1, t_2) space. The efficient spiral sampling of the k-space enables the acquisition of a single-slice 2D COSY dataset with an 8×8 matrix in 8:32 min on 3T clinical scanners, which makes it feasible for *in-vivo* studies on human subjects. Here we present the first results obtained on phantoms, human volunteers and patients with brain tumors. The patient data obtained by us represent the first clinical demonstration of a feasible and robust multivoxel 2D COSY. Compared to the 2D J-resolved method, 2D COSY and TOCSY provide increased spectral dispersion which scales up with increasing main magnetic field strength and may have improved ability to unambiguously identify overlapping metabolites. It is expected that the new developments presented in this work will facilitate *in-vivo* application of 2D chemical shift correlation MRS in basic science and clinical studies.

Keywords

*Address correspondence/reprints request to: Ovidiu C. Andronesi, Athinoula A. Martinos Center for Biomedical Imaging, Massachusetts General Hospital, Harvard Medical School, 149 Thirteenth Street, Suite 2301, Boston, MA 02129, USA; ovidiu@nmr.mgh.harvard.edu, oandronesi@gmail.com.
#These authors contributed equally.

1. INTRODUCTION

Spectrally two-dimensional (2D) chemical shift correlation MR spectroscopy (MRS) methods, such as COSY (Correlation Spectroscopy, (1)) or TOCSY (Total Correlation Spectroscopy, (2)) can help to unambiguously identify overlapping metabolites. Currently, *in-vivo* 1D MRS includes contribution from 18 metabolites (3), however *ex-vivo* 2D MRS on intact tissue biopsies (4,5) distinguish more than 30 metabolites. Besides resolving overlapping peaks such as lactate / lipids, glutamate / glutamine / GABA, and total choline (Choline / Phosphocholine / Glycerophosphocholine), *in-vivo* 2D COSY or TOCSY could identify new metabolites of interest in normal physiology and disease.

Scalar coupled spins are allowed to exchange magnetization during a so called mixing period in COSY and TOCSY experiments. While for COSY (1) the mixing happens during the t_1 evolution which is free of RF pulses, for TOCSY (2) the mixing period is realized under the action of a train of RF pulses right after t_1 evolution. The train of RF pulses in TOCSY is used to average out the chemical shift interaction and create an average Hamiltonian that contains only the isotropic scalar coupling interaction. Hence, spins can exchange magnetization over multiple bonds in TOCSY (6), while in COSY (7) only direct scalar coupled spins exchange magnetization. This is achieved at the cost of increased RF power deposition in TOCSY. For assignment purposes in homonuclear spin systems, TOCSY experiment is one of the most powerful methods because: i) it obtains the full correlation matrix (direct and relay crosspeaks) of the spin network, while COSY provides only direct correlations; and ii) pure absorptive phase-sensitive crosspeaks are obtained in TOCSY, while COSY exhibits crosspeak multiplets with equal positive and negative intensities leading to zero integrated intensity in phase-sensitive spectra, or to partial signal cancellation and increased linewidths in magnitude mode spectra. In particular the last aspects could be important for *in-vivo* applications. Compared to 2D J-resolved spectra (8) that resolve overlapped signals along a second and fixed scalar coupling dimension (limited to ±15 Hz for ^1H), 2D COSY and TOCSY provide increased spectral dispersion along a second larger chemical shift dimension which scales up to kHz with increasing main magnetic field strength, B_0.

To date, most *in-vivo* localized 2D COSY data have been recorded as single voxel (L-COSY (9), CT-COSY (10)), and there is limited progress reported towards a feasible multivoxel implementation (11–17). *In-vivo* 1D spectral-editing TOCSY has been shown previously (18,19), and localized 2D TOCSY (20) was recently demonstrated, but only as single-voxel methods. However, single-voxel techniques represent a serious limitation, and expanding the spatial coverage is highly desirable for clinical applications, as a control voxel in a healthy area is often needed in addition to the voxel in pathological region of interest. Due to inherently long acquisition times of 2D COSY or TOCSY, their multivoxel implementation is difficult to realize within feasible limits of *in-vivo* scan times using conventional phase encoding (11,12). Hadamard spectroscopy (14), ultrafast low-angle rapid acquisition with relaxation enhancement (15), multiple spin-echoes (16) and EPI (13,17) acquisitions have been proposed to shorten scan time of multivoxel COSY (named correlation peak imaging in Ref. (11)). In particular, spectroscopic methods using multiple spin-echoes (21,22) and PEPSI (23,24) acquire simultaneously one spatial dimension and one frequency dimension. However, scan times of multivoxel 2D COSY based on these methods are still too long (25–30 min for brain) for many clinical applications.

In this work we propose the broader concept of correlation chemical shift imaging (CCSI) which includes both 2D COSY and 2D TOCSY imaging experiments. We show that CCSI can be performed *in-vivo* by robust experiments in feasible amounts of time on human brain.

Compared to previous approaches of multivoxel COSY (11–17), our method uses an improved adiabatic localization and a time efficient spiral spatial encoding.

We used low power optimized adiabatic sequences to excite the signal in COSY and TOCSY experiments. These are based on 2D COSY-LASER and Z-TOCSY-LASER pulse sequences that were previously demonstrated in single voxel experiments (20). Here we extended their use for the purpose of CCSI. We make use of constant-density spiral trajectories that simultaneously encode two spatial dimensions and one frequency dimension. The spiral sampling of k-space in spectroscopic imaging (25–28) has been shown previously to make feasible the acquisition of multivoxel 2D J-resolved (29,30), and CT-PRESS homonuclear decoupled (31) spectra on human subjects.

2D-spectral/2D-spatial data obtained on 3T and 1.5T clinical scanners for phantoms, healthy volunteers and patients with brain tumors are presented. In particular, adiabatic 2D COSY spiral imaging at 3T can be obtained in 8:32 min with adequate signal to noise ratio (SNR) in human brain scans for a single slice of 8×8 matrix, 2×2 cm^2 in plane resolution, 2.5 cm slice thickness, and 10 ml voxel volume. *In-vivo* adiabatic 2D TOCSY spiral imaging is demonstrated on healthy volunteers at 1.5T using the same acquisition matrix and voxel size. Data obtained by us on volunteers and phantoms represent the first example of TOCSY imaging, while patient data represent the first clinical demonstration of a feasible and robust multivoxel 2D COSY.

2. THEORY

In CSI experiments pre-selection of a large volume of interest (VOI) is obtained using slice selective pulses which are applied in three orthogonal directions, such as in the case of PRESS (32), STEAM (33) and LASER (34) sequences. Constant adiabaticity gradient modulated GOIA-W(16,4) pulses (35) and LASER are optimal for selection of VOI by providing: 1) precise localization with negligible chemical shift displacement error (CSDE), uniform flip angle excitation of VOI, and no lipid contamination from subcutaneous fat; 2) efficient mixing for scalar coupled spins over a large bandwidth (BW); and 3) reduced power deposition or specific absorption rate (SAR).

CSDE is inversely proportional with BW of slice selective pulse (*CSDE* ~1/*BW*), thus increasing pulse BW is effective in reducing CSDE. For conventional pulses BW is limited by the maximum B_1 available, however, adiabatic pulses can obtain very large BW when B_1 is limited. GOIA-W(16,4) pulses (35) can achieve 20 kHz bandwidth with 0.81 kHz (18.7 μT) maximum B_1 field. With a BW of 20 kHz a negligible 2% CSDE is obtained over 3.5 ppm ^{1}H chemical shift range at 3T. By comparison, Mao refocusing pulses (36) that are typically used in L-COSY (9) can have up to 38% CSDE over a 3.5 ppm ^{1}H chemical shift range at 3T (35). By design, GOIA pulses (37) also have the advantage of a constant adiabatic factor over entire BW, while for conventional adiabatic pulses the adiabatic factor decreases away from center frequency. In addition to minimizing CSDE, GOIA-W(16,4) pulses provide optimal flip angles uniformly across large VOI and spectral bandwidth (SW), which is especially important for enabling efficient coherence transfer among scalar coupled spins. A comparison between VOI localized with LASER, PRESS, L-COSY and STEAM is included in Supplementary Information (Fig. S1).

In 2D COSY-LASER (Fig. 1) sequence GOIA-W(16,4) pulses are used only for localization. For 2D Z-TOCSY-LASER (Fig. 1) sequence GOIA-W(16,4) pulses are used for magnetization transfer between scalar coupled spins during MLEV-16 mixing block, and for localization within LASER block. Low SAR of GOIA-W(16,4) allows short repetition times (TR) for 2D COSY-LASER (TR = 1s at 3T) and Z-TOCSY-LASER (TR = 2s-3s at 3T) sequences (20). Details of the 2D-spectral/2D-spatial CCSI pulse sequences (COSY-

LASER-SPIRAL and TOCSY-LASER-SPIRAL) are given in the Figure 1 and in the Methods section.

In particular, adiabatic longitudinal mixing for TOCSY has been shown by quantum mechanical simulations and experiments (20) to be more efficient than adiabatic transverse mixing (19). The Hamiltonian of TOCSY mixing under MLEV-16 scheme (38) using GOIAW(16,4) pulses in the case of a two scalar coupled spins is given by

$$\widehat{H}(t)=-\Omega_1\widehat{I}_{z,1}-\Omega_2\widehat{I}_{z,2}+J\left[\widehat{I}_{x,1}\widehat{I}_{x,2}+\widehat{I}_{y,1}\widehat{I}_{y,2}+\widehat{I}_{z,1}\widehat{I}_{z,2}\right]+\sum_{k=1}^{N_p}\gamma\left\{B_{1,k}(t)\left[\widehat{F}_x\,\cos\,(\varphi_\mathbf{k}(\mathbf{t}))+\widehat{\mathbf{F}}_\mathbf{y}\,\sin\,(\varphi_\mathbf{k}(\mathbf{t}))\right]+zG_k(t)\widehat{F}_z\right\}$$

[1]

assuming N_p (multiple of 16) gradient modulated adiabatic pulses with $B_{1,k}(t)$ amplitude modulation, $\varphi_k(t)$ phase modulation, $G_k(t)$ gradient modulation ($k=\overline{1,N_p}$), and Ω_n (n = 1,2) and J represent chemical shifts and scalar coupling, respectively (in frequency units), $\hat{I}_{\alpha,n}$(α = x,y,z; n = 1,2) denote individual spin operators, and $\hat{F}_\alpha$ ($\alpha = x,y,z$) total spin system operators ($\hat{F}_\alpha = \hat{I}_{\alpha,1} + \hat{I}_{\alpha,2}$). The Hamiltonian of COSY can be obtained simply from Eq. [1] by removing the RF term. In the case of most mobile metabolites the influence of anisotropic interactions such as chemical shielding anisotropy and dipolar couplings on coherent evolution of the spin system can be neglected.

RF pulses with a constant adiabatic factor (Q) can be obtained if modulation functions fulfill the condition (37,39)

$$\varphi_k(t)=2\pi\frac{1}{Q}\int_0^t\left[G_k(\tau)\int_0^\tau\frac{\gamma B_{1,k}^2(\tau')}{G_k(\tau')}d\tau'\,-\,\omega_c\right]d\tau+\varphi_k(0)$$

[2]

, where ω_c is the center sweep frequency and $\varphi_k(0)$ represents the initial phase of the pulse, which in our case follows MLEV-16 scheme (i.e. $\varphi_k(0) = 0$ if k = 1,2,5,8,11,12,14,15 and $\varphi_k(0) = \pi$ if k = 3,4,6,7,9,10,13,16). The $B_1(t)$ and $G(t)$ modulations are defined in (37) and are based on WURST function (40).

The coherent spin evolution under the Hamiltonian of Eq. [1] is determined by Liouville-von-Neumann equation of motion for spin density matrix (41)

$$\frac{d}{dt}\widehat{\sigma}(t)=-\frac{i}{\hbar}\left[\widehat{H}(t),\widehat{\sigma}(t)\right]$$

[3]

, which has formal solution

$$\widehat{\sigma}(t)=\widehat{U}(t)\widehat{\sigma}(0)\widehat{U}^{-1}(t)$$

[4]

, with propagator $\widehat{U}(t)=T \exp\left[-i/\hbar \int_0^t \widehat{H}(\tau)d\tau\right]$, and T is the Dyson time-ordering operator. In the case of time periodic perturbations such as MLEV-16, the propagator over a full period of mixing time (t_{mix}) can be expanded by Average Hamiltonians Theory (AHT, (42)) into a series

$$\widehat{U}(t_{mix})=\exp\left[-i/\hbar\left(\widehat{\overline{H}}^{(0)}+\widehat{\overline{H}}^{(1)}+\widehat{\overline{H}}^{(2)}+\cdots\right)t_{mix}\right]$$

[5]

where the first order average Hamiltonian $\widehat{\overline{H}}^{(0)}=1/t_{mix}\int_0^{t_{mix}}\widehat{H}(t)dt$ is consider to have the most important contribution, and higher order terms are often included only as corrections. The aim of MLEV-16 scheme is to remove the influence of chemical shift and create an average Hamitonian that in the first order contains only scalar coupling interaction $\widehat{\overline{H}}^{(0)}=J\widehat{I_1}\widehat{I_2}$. The amplitude of the RF field needs to exceed a certain threshold to obtain this ideal average Hamiltonian. In practice, for RF fields that are feasible *in-vivo* on humans a somewhat weaker average Hamiltonian is obtained $\widehat{\overline{H}}^{(0)}=J_{eff}\widehat{I_1}\widehat{I_2}$ with a smaller effective scalar coupling constant $J_{eff} \leq J$. We have shown this effect through numerical simulations of TOCSY buildups (Fig. 2A,B).

TOCSY crosspeaks buildup curves can be simulated assuming that initially only one of the spins has magnetization (i.e. initial density matrix $\hat{\sigma}(0) = \hat{I}_{z,1}$ for longitudinal mixing) and detecting magnetization transferred on the second spin ($\langle\hat{I}_{z,2}\rangle = Tr\{\hat{\sigma}(t_{mix})\hat{I}_{z,2}\}$) for increasing mixing times (t_{mix}). In practice numerical integration of Eq. [4] offers an easier approach than analytical tools, such as Average Hamiltonian Theory (42) or Floquet Theory (43), that are needed for solving Eqs. [3–4] with a time dependent Hamiltonian. Buildup curves at 1.5T and 3T under MLEV-16 with GOIA-W(16,4) pulses of 2ms and 1.5ms durations are shown in Figure 2 for the case of a lactate spin system. Incoherent relaxation mechanisms were not included explicitly in these buildups.

COSY buildups can be simulated similarly by considering $\hat{\sigma}(0) = \hat{I}_{x,1}$ and $\langle\hat{I}_{x,2}\rangle = Tr\{\hat{\sigma}(t_{mix})\hat{I}_{x,2}\}$, under the time constant Hamiltonian that contains only chemical shift and scalar coupling interactions. COSY buildup curves at 1.5T and 3T were simulated by omitting RF part from Hamiltonian of Eq. [1].

Spiral spectroscopic imaging (25,26) trades off spatial resolution with spectral bandwidth. Given spatial resolution requirements and physical limitations of gradient hardware on clinical scanners it is impossible to encode all spatial information with a spiral trajectory of length less than, or equal to Δt_2 (0.833 ms for SW of 1.2 kHz). Hence, interleaved spiral trajectories ($N_{interleaves} = N_a * N_t$) are necessary, which typically are decomposed into so-called angular (N_a) and temporal (N_t) interleaves. The desired field of view (FOV), spatial resolution (matrix size) and SW are obtained by modifying the duration of each spiral lobe concomitant with the number of angular interleaves (for FOV, spatial resolution) and the number of temporal interleaves (for SW). Angular interleaving decompose the (k_x,k_y) space into sparser N_a spiral trajectories rotated by $\theta_n=(n-1)2\pi/N_a \cdot (n=\overline{1, N_a})$. For temporal interleaving, the readout gradients start $(n-1)\Delta t_2$ seconds $(n=\overline{1, N_t})$ later relative to the ADC acquisition. The choice of temporal or angular interleaves is made such that acquisition time (N_a*N_t*TR) is minimized. A rewinder gradient is used after each spiral gradient to return to the origin of k-space, the duration of the rewinder being fixed to the

shortest value. In order to estimate spatial encoding of spiral trajectories, simulations of point spread function (PSF) were performed and are shown in Figure 3.

3. METHODS

3.1. Numerical simulations

Quantum mechanical simulations were performed in GAMMA (44) for buildup curves of crosspeaks under TOCSY mixing with MLEV-16 and GOIA-W(16,4) pulses, and for COSY omitting RF part from the Hamiltonian of Eq. [1]. A two spin system was considered to have lactate's chemical shifts and scalar coupling ($\Omega_1 = 1.3$ ppm, $\Omega_2 = 4.1$ ppm, $J = 6.93$ Hz from Ref. (45)). Buildup curves were simulated for two main magnetic fields B_0 at 1.5T and 3T, which are clinically the most common. Typically, the maximum possible RF amplitude ($\gamma B_{1,max}$) does not exceed 1kHz for body coils on clinical scanners. Hence, for TOCSY we investigated two GOIAW(16,4) pulses designed to have the minimum (R = 20) adiabatic factor and specific absorption rate (SAR) for in-vivo use: i) duration Tp = 2 ms, bandwidth BW = 10 kHz, $\gamma B_{1,max} = 0.76$ kHz, and ii) Tp = 1.5 ms, BW = 13.34 kHz, $\gamma B_{1,max} = 1.02$ kHz. These buildups were compared with the ideal buildup when chemical shifts are neglected and only scalar coupling is considered. In all simulations spin evolution was calculated using a piece-wise constant Hamiltonian with a time step of 20 µs, as detailed in Ref. (20). Symmetry of pulse shapes and periodicity in spin evolution were exploited to speed-up calculations.

Point spread functions were simulated in Matlab (The MathWorks, Inc., Natick, MA, USA) for constant density spiral trajectories that were used to acquire FOV = 160×160 mm^2 and SW = 1.2 kHz with two matrix sizes of 8×8 and 16×16, respectively. The spiral gradient waveforms that were generated on the scanner during sequence preparation were exported and numerically integrated. Hardware infidelities and possible experimental deviations from theoretical gradient waveforms were not taken into account.

3.2. Hardware and sequence programming

All measurements were done on 3T Tim Trio or 1.5T Avanto systems (Siemens, Erlangen, Germany), using body coil for transmission and a 32-channel head phased receive array. The maximum amplitude of B_1 field delivered by the transmit body coil is limited to 1 kHz (23.4 µT). The gradient system specifications include a maximum nominal amplitude of 26 mT/m and a maximum slew rate of 170 mT/(m·ms).

For both COSY and TOCSY experiments VOI was selected along three orthogonal spatial dimensions with a symmetric LASER localization employing GOIA-W(16,4) pulses (35) with duration of 3.5 ms, BW of 20 kHz, and $B_{1,max}$ of 0.817 kHz. Gradient spoilers of 10 mT/m and 8 mT/m, 1.58 ms total duration (540 µs ramp-up/down times, 500 µs flat top) were placed around slice selective pulses on all gradient channels. The minimum LASER echo time (TE) that can be obtained with these parameters is 40 ms. Amplitude, gradient and phase modulations of GOIA-W(16,4) were implemented in the scanner sequence software (VB17A) according to Ref. (35).

TOCSY mixing was performed with GOIA-W(16,4) pulses of 2 ms, 10 kHz BW and 0.76 kHz $B_{1,max}$ following an MLEV-16 scheme (20). To enable longitudinal mixing a gradient enhanced z-filter was employed using 90° pulses and spoiler gradients of 3 ms total duration, 500 µs ramp-up/down times, and 11.5 mT/m amplitude, surrounding MLEV-16 block. Due to z-filter, the mixing time does not contribute to the echo time. TOCSY mixing time was set to 64 ms ($N_{mix} = 2$) for phantom experiments at 3T, and to 32 ms ($N_{mix} = 1$) for human volunteer measurements at 1.5T. All 90° pulses used in TOCSY or COSY were non-selective BIR-4 (46) adiabatic pulses (4 ms duration, 10 kHz bandwidth).

Selection of coherence transfer pathway (CTP) was performed with sine-bell shaped gradients of 1 ms duration and 11.5 mT/m amplitude. Phase sensitive spectra can be obtained with an echo-antiecho acquisition by changing the polarity of the CTP gradients in separate t_1 increments, and in the case of TOCSY the phase of the first 90° z-filter pulse is simultaneously alternated x to −x (47).

No outer volume suppression (OVS) was necessary on phantoms or human subjects due to precise LASER pre-localization (35). Water suppression was realized with a WET scheme (48) in all sequences.

For 2D spectra, the time interval after the first 90° excitation pulse was incremented in consecutive experiments to realize t_1 evolution. A time increment of 0.833 ms was used, corresponding to approximately 10 ppm (SW of 1.2 kHz at 3T) for f_1 (indirect) frequency dimension, and 64 t_1 increments were recorded in four-dimensional (k_x,k_y,t_1,t_2) space. While all sequences are single shot and can be run as such, a minimum phase cycle of two steps for the first 90° excitation pulse improves spectra quality by removing axial peaks and t_1 noise coming from water signal that starts to recover during t_1 evolution. Since averaging for SNR is typical, a minimum phase cycle is not a problem, and 4 averages were added for *in-vivo* experiments. Eight dummy scans were used only before the first t_1 increment, to allow for T1 relaxation and reach a steady-state magnetization.

Spiral waveforms ($N_{spirals}$ = 380) were played on the read and phase gradient channels for spectroscopic imaging of LASER pre-localized VOI. Spectral bandwidth for f_2 (direct) frequency dimension was set to 1.2 kHz (Δt_2 of 0.833 ms), which roughly corresponds to 10 ppm at 3T. Two CCSI spatial resolutions were tested: 1) field of view (FOV) 16×16 cm^2, 8×8 in-plane resolution matrix, 2×2 cm^2 in-plane voxel size; 2) FOV 16×16 cm^2, 16×16 in-plane resolution matrix, 1×1 cm^2 in-plane voxel size. In all cases a 2.5 cm slice thickness has been used. Constant-density spiral-out trajectories were designed (49) so that the number of interleaves was: i) $N_{interleaves}$ = 2 for 8×8 matrix (N_a = 1, N_t = 2), and ii) $N_{interleaves}$ = 6 for 16×16 matrix (N_a = 3, N_t = 2). An acquisition time of 8:32 min can be achieved when recording 64 t_1 increments with 4 averages (NA) for 8×8 matrix, and 12:48 min when recording 64 t_1 increments with 2 averages for 16×16 matrix, assuming a repetition time (TR) of 1s. Spiral trajectories are more time efficient than multiple spin-echoes or EPI. By comparison, for a slice of 8×8 matrix of voxels the spiral encoded CCSI can be 8 times faster than multi echo (employing four spin echoes) and 4 times faster than EPI encoded versions (assuming the same repetition times, number of averages, and t_1 increments). In addition, spiral gradient waveforms have a smoother variation and are less demanding than EPI for gradient hardware in terms of maximum amplitude, rise time and slew rate.

The maximum gradient and slew rate used in spirals' design were set to conservative levels, 9.8 mT/m and 120 mT/m/ms, respectively, in order to avoid any kind of gradient fidelity issues. The length of rewinder gradient was not more than 15% of the total duration of the spiral lobe. Gradient delays between ADC and x and y gradients were measured to be 8μs, and were corrected for in the reconstruction.

3.3. CCSI of phantoms

Three phantoms were used to test localization and SNR: i) a large homogenous phantom (16 cm diameter) containing only brain metabolites at physiological concentrations for NAA 8 mM, glutamate (Glu) 6 mM, GABA 1 mM, choline (Cho) 5 mM, creatine (Cre) 3 mM, myoinositol (Myo) 4mM, and lactate (Lac) 1 mM; ii) a double-layer phantom consisting of an outer layer (2 cm thick) of oil and an inner core (8 cm diameter) of brain metabolites (the same like in phantom 1); iii) a phantom with two compartments (6 cm diameter each),

containing one compartment filled with GABA solution (5 mM) and the other compartment with lactate solution (50 mM).

CCSI employing COSY-LASER-SPIRAL and TOCSY-LASER-SPIRAL sequences were performed on all three phantoms at 3T. For each sequence, both 8×8 ($N_{interleaves}$ = 2, NA=4) and 16×16 ($N_{interleaves}$ = 6, NA=2) matrix were tested to acquire FOV = 16×16 cm^2 and SW = 1.2 kHz. A TR of 1s was used for COSY-LASER-SPIRAL. Due to higher SAR, a TR of 1.75s was employed for TOCSY-LASER-SPIRAL.

3.4. CCSI of human subjects

CCSI of human brain was collected on six healthy volunteers (30 years median age) and three patients with brain tumor (Glioblastoma multiforme, GBM, 45 years median age). The studies with human subjects were approved by the IRB of our institution.

A minimum TR of 1s with COSY-LASER-SPIRAL was possible on all human subjects at 3T. Because of higher SAR, a minimum TR in the range of 2s–3s would be necessary for TOCSY-LASER-SPIRAL on human subjects at 3T (20). Because of slower buildup curves, longer TR and longer associated scan times at 3T for TOCSY-LASER-SPIRAL, only COSY-LASER-SPIRAL sequence was tested in vivo at 3T. TOCSY-LASER-SPIRAL was demonstrated on human volunteers at 1.5T where faster buildups provide increased crosspeaks for shorter mixing times and SAR constrains allows a TR of 1.5s or shorter. A total acquisition time of less than 10 minutes was considered as desirable for human CCSI, and this can be achieved at 3T with COSY-LASER-SPIRAL that acquires a 8×8 matrix ($N_{interleaves}$ = 2), 64 t_1 increments, NA = 4, and TR = 1s in a total time of 8:32 min. The same matrix was used for TOCSY-LASER-SPIRAL on human volunteers at 1.5T, but acquiring 50 t1 increments, NA = 12 and TR = 1.5s in 30 min. The TOCSY mixing time was set at 32ms for measurements on human subjects at 1.5T. The RF amplifiers of the Avanto systems drain for mixing times longer than 32 ms and trigger an execution error, while RF amplifiers of 3T Tim Trio allow mixing times of up to 100 ms. As shown in simulations TOCSY buildups are faster at 1.5T, and 32 ms mixing yield detectable crosspeaks for most metabolites. In all experiments FOV of 16×16 cm^2 and a slice thickness of 2.5 cm were chosen, yielding voxels of 10 ml (2×2 cm^2 in-plane resolution) which was found to be the minimum voxel volume for adequate SNR of COSY with acquisition times shorter than 10 min.

Images used to position VOI of CCSI were acquired with: i) MEMPRAGE (50) sequence (TR = 2.53 s, TE1/TE2/TE2/TE3/TE4 = 1.64/3.5/5.36/7.22 ms, TI = 1.2 s, 1 mm^3 isotropic) for volunteers; ii) MEMPRAGE acquired post-Gd (Magnevist) contrast i.v. injection in tumor patients. B_0 shimming over the entire VOI was performed using the Siemens advanced shimming routine until a line width of 15 Hz (magnitude mode) or better was obtained for the water signal.

3.5. Processing of the CCSI data

Spiral data from separate receive coils were 2D gridded on a Cartesian grid for FFT (Fast Fourier Transformation) using Kaiser-Bessel kernel (51), and the data from all 32 coil elements were combined using complex coil weights obtained from a short prescan. No window function was applied for k-space. Data were zero filled to 512 points in the t_2 dimension prior to FFT. For each t_1 increment (all 64 (k_x,k_y,t_2) sub-spaces) reconstruction along spatial (x,y) and f_2 frequency dimension was implemented in the Siemens Image Calculation Environment (ICE), and viewing of the reconstructed 1D spectra was therefore possible online at the Siemens scanner console. The grid of 1D spectra corresponding to the first t_1 increment was always inspected for quality assurance. All t_1 increments acquired on

the 8×8 matrix were interpolated to 16×16 matrix by the on-line ICE reconstruction program. However, 2D spectra analysis was performed on the original 8×8 acquisition matrix by summing the signal of each 4 neighboring voxels. The matrix of 16×16 data was not modified, and was kept the same for 1D and 2D reconstruction.

Reconstruction along f_1 frequency dimension was performed off-line in Matlab. The DICOM files of each t_1 increment were exported off-line and loaded into Matlab for FT along f_1 frequency dimension. Due to heavy signal truncation along t_1 dimension, linear prediction is mandatory prior to FT in order to reduce large ringing ridges along f_1 spectral dimension. Linear prediction forward to 128 points along f_1 using the ITMPM method (Information Theory and the Matrix Pencil Method, (52)) has been employed. A shifted square-sine window function was employed in both f_1 and f_2 dimensions in order to improve crosspeaks, reduce ringing and baseline distortion. The 2D spectra were displayed as contour levels in magnitude mode, with the first contour level chosen three times floor noise level as estimated from standard deviation of baseline in a signal free spectral region (0.5ppm-0ppm/0.5ppm-0ppm).

4. RESULTS

4.1. Simulations

Simulated buildup curves for crosspeaks of TOCSY and COSY experiments at 3T and 1.5T are shown in Figure 2. In general, as mentioned in the theory part, lower RF fields provide slower TOCSY buildups. Ideal TOCSY buildup curves can be obtained for RF amplitudes above threshold values of 1.5 kHz at 3T and 1.1 kHz at 1.5T, which are slightly larger than the 1 kHz maximum RF amplitude deliverable by the body transmit coil. In the case of TOCSY at 3T (Fig. 2A), longitudinal mixing with $B_{1,max} = 0.75$ kHz exhibits a buildup rate which is half of the ideal buildup rate obtained if only scalar coupling is considered. Approximately 50% transfer can be obtained for a mixing time of 64 ms. An increase to the maximum available RF amplitude ($B_{1,max} = 1$ kHz) provides a significantly faster buildup, improving transfer efficiency to approximately 80% at 64 ms mixing time. The differences are explained by the fact that larger RF field amplitudes averages-out more effectively the unwanted chemical shift interaction in the first order average Hamiltonian, resulting in a stronger effective scalar coupling constant (J_{eff}). In experimental testing, efficiency of mixing at higher RF increased only slightly, which could be related to the fact that the RF amplifier can not sustain required amplitude for the entire duration of mixing period. TOCSY buildups at 1.5T (Fig. 2B) are much closer to the ideal buildup, having 90% efficiency at 64 ms mixing for $B_{1,max} = 0.75$ kHz, owing to the two-fold reduction of chemical shift interaction. Mixing 32 ms at 1.5T provides similar efficiency as mixing 64 ms at 3T using $B_{1,max} = 0.75$ kHz in the case of the two spin system of lactate. Performing TOCSY experiment at 1.5T with 32 ms time mixing has the advantage of a decreased SAR deposition.

COSY buildups were simulated for the same spin system at 3T (Fig. 2C) and 1.5T (Fig. 2D). The situation when only scalar coupling is considered provides the same buildup as in the case of TOCSY. When chemical shifts are included, fast oscillations superimpose on the scalar coupling buildup due to transverse mixing of COSY. However, the maximum transfer occurs at the same position in all buildups (approx. 64 ms mixing time).

Point spread functions for spirals designed to acquire 8×8 and 16×16 matrixes over FOV = 16×16 cm^2 and SW = 1.2 kHz are shown in Figure 3. One angular interleave is necessary for 8×8 matrix (Fig. 3A), while three angular interleaves are used for 16×16 matrix (Fig. 3B). Good spatial localization is noticed for both matrixes. Although 8×8 matrix represents a coarse spatial coverage, the associated PSF (Fig. 3C) has a well defined main lobe with a

full width at half maximum (FWHM) of 2 cm and the baseline ringing does not indicate considerable voxel bleeding. The ratio between the first positive sidelobe and the main lobe is 2.6%. Similar results are obtained for PSF of 16×16 matrix (Fig. 3D) that has, as expected, a two fold narrower main lobe (FWHM = 1 cm). The largest signal contamination and voxel bleeding could come from subcutaneous lipids, however this possibility is eliminated by the sharp excitation profile of LASER as shown in Supplementary Information (Figs. S1 and S2). *In-vivo* data confirm these findings in both volunteers and patients.

4.2. Phantom data

Several aspects of CCSI were investigated at 3T on three phantoms: 1) uniformity of excitation and SNR of 2D MRS in the uniform phantom; 2) LASER pre-localization of VOI and lipid contamination in the double-layer phantom; 3) spatial encoding of spiral trajectories in the two-compartment phantom. Experiments on phantoms have been performed to choose meaningful starting parameters for *in-vivo* measurements. The results obtained on the double-layer and the two-compartment phantoms are shown in Supplementary Information (Figs. S2 and S3).

In Figure 4 results obtained on the uniform phantom containing brain metabolites at physiological concentrations are shown. A VOI (blue rectangle, 10×10 cm^2 in plane, 2.5 cm thickness) was selected by LASER. Two in plane resolutions of 1×1 cm^2 (16×16 matrix, FOV = 16×16 cm^2) and 2×2 cm^2 (8×8 matrix, FOV = 16×16 cm^2) were tested in order to investigate the SNR limits and optimize acquisition parameters for *in-vivo* experiments. We found that a voxel size of 10 ml ($2\times2\times2.5$ cm^3) was necessary for adequate SNR if the acquisition times were to be shorter than 10 minutes. Spectra recorded with both COSY-LASER-SPIRAL and TOCSY-LASER-SPIRAL sequences are included.

Crosspeaks of all metabolites are well visible and separated from the main diagonal. Due to coherent transfer of in-phase longitudinal magnetization in TOCSY the multiplet structure of each crosspeak is more apparent in TOCSY spectra than in COSY. Transfer over multiple bonds is possible in TOCSY and relay crosspeaks are visible in TOCSY spectra which can not be obtained in COSY (see also Fig. 3 in Supplementary Information). To illustrate SNR of 2D MRS, projections along f_1 and f_2 spectral dimensions are shown for lactate crosspeak. Due to transfer of in-phase and anti-phase magnetization, partial signal cancellation can be noticed for COSY as a notch in the middle of the crosspeak along f_2 projection, and slightly larger linewidths for COSY crosspeaks is noticed in both f_1 and f_2 projections (see also enlarged crosspeaks in Fig. S4 from Supplementary Information). The expected CH multiplet structure of Lactate is clearly noticed in the f2 projection from TOCSY. 1D spectrum of the first t1 increment from the same voxel is included for comparison. A quantitative analysis is presented in Tables 1 and 2.

4.3. Human data

CCSI measured at 3T on the brain of a healthy volunteer with COSY-LASER-SPIRAL sequence is shown in Figure 5. Spectra are acquired in 8:32 min, using parameters tested on the uniform brain phantom. LASER selects a large VOI (8×8 cm^2, blue rectangle) in centrum semiovale above the ventricles, which includes the central 4×4 voxels of FOV (yellow rectangle). Example of a representative 2D spectrum from a central voxel (red outlined) shows clear crosspeaks which correspond to NAA, glutamate, GABA, choline, glycerophosphocholine (GPC), phosphocholine (PC), phosphoethanolamine (PE), myoinositol, and threonine (Thr). Projections along f_1 and f_2 spectral dimensions through glutamate crosspeak are indicative of SNR and quality of data. 1D spectrum of the first t1

increment from the same voxel is shown for direct visual comparison. Tables 1 and 2 contain the quantitative analysis.

TOCSY-LASER-SPIRAL spectra measured at 1.5T on a healthy volunteer are shown in Figure 6. The size and position of FOV (yellow rectangle) and VOI (blue rectangle) were chosen the same like for COSY volunteer. Crosspeaks corresponding to aspartate (Asp), NAA, glutamate, choline, myoinositol, and threonine are clearly seen. Crosspeaks of GPC, PC, PE were not detected, presumably due to shorter 32 ms mixing time. In a previous (20) single voxel implementation of TOCSY at 3T the crosspeaks of GPC were observed for 64 ms mixing time. f_1 and f_2 projections through glutamate crosspeak, and 1D spectrum of the first t1 increment show the quality (SNR, baseline) of data. For all metabolites, crosspeaks are well above noise level, and the quantitative estimation is presented in Tables 1 and 2.

Figure 7 demonstrates results obtained at 3T from a patient with glioblastoma. The same acquisition parameters as in the volunteer case are used to acquire COSY-LASER-SPIRAL spectra. The two tumor regions visible in contrast enhanced T1 weighted image can be identified also in 2D spectra. Characteristic for the tumor regions are large lipid (Lip) signals suggestive of underlying necrosis. However, the high lipid signals do not contaminate visibly the neighboring voxels through PSF ringing.

An overlay of 2D COSY spectra originating in a tumor region (red spectrum) and in a healthier region (blue spectrum) is shown. The tumor spectrum represents a good example of COSY being able to resolve overlapping metabolite signals such as lipids and lactate. In the corresponding 1D spectrum shown below, lipid and lactate signals overlap completely.

Interestingly, while NAA is absent as expected, aspartate signal is detected in tumor by in-vivo 2D MRS, which could be related to tumor biology. This is in line with our previous findings (53) from high quality *ex-vivo* 2D high resolution magic-angle-spinning (HRMAS) spectra of intact glioblastoma biopsies. Choline, GPC, PE and myoinositol are identified in the tumor spectrum, though they do not seem to be enhanced compared to the healthy spectrum. This is evident also by comparing the total choline peak in the 1D spectra. A distinct crosspeak (X) seems to be present at 3.6/2.3 ppm (f_2/f_1) in the tumor spectrum which could match the Hα-Hβ correlation for valine. However, this assignment can be made only tentatively since the Hβ-Hγ correlations of valine are not seen. The high signal at ~0.9 ppm in the methyl region of the 1D spectrum could be suggestive of contribution from metabolites containing methyl groups such as valine.

4.4. Quantitative analysis

Quantitative analysis of SNR is provided in Table 1 for each sequence in phantoms and volunteers. In phantoms SNR of crosspeaks is greater than 20 for all metabolites. In volunteers the minimum SNR of COSY crosspeaks at 3T is approximately 10, while the minimum SNR of TOCSY crosspeaks at 1.5T is 8. The SNR of crosspeaks relative to the SNR of diagonal peaks is indicative of the sensitivity of the 2D MRS compared to the 1D MRS. The largest difference is observed for NAA and Cho, which is explained by the fact that considerable more protons contribute to the main diagonal peaks of NAA (2.01 ppm) and Cho (3.19 ppm) compared to their crosspeaks, NAA (4.38/2.67 ppm) and Cho (4.05/3.5 ppm). For other metabolites that do not have uncoupled methyl groups giving rise to intense singlet diagonal peaks, the SNR of crosspeaks compares more favorably to the SNR of diagonal peaks, ranging between 13% and 70%. In general SNR of TOCSY compared to SNR of COSY is lower (47% to 77% in phantoms), with the exception of lactate which has a better SNR in TOCSY.

Volumes of individual crosspeaks and diagonal peaks are given in Table 2. Concentration of each metabolite can be estimated from the volumes of the corresponding crosspeaks and a calibrated reference signal. Comparison between volumes of crosspeaks and diagonal peaks needs to take into account the number of protons contributing to the formation of crosspeak or diagonal peak, the mixing time, and the buildup rate of crosspeaks. With these corrections, similar metabolite ratios are found when using crosspeak volumes or diagonal peak volumes. For *in-vivo* 2D MRS quantification, often the ratio of the metabolite crosspeak volume to the creatine diagonal peak volume is reported (9), and the volume of diagonal peak of creatine is included in Table 2.

5. DISCUSSIONS

In-vivo 2D-spectral/2D-spatial MRS has tremendous potential to improve our ability to characterize metabolism under normal physiological and disease conditions by disentangling overlapped spectra or uncovering new metabolites that are typically obscured in one-dimensional spectroscopy. However, this method faces difficult challenges related to limited spatial coverage and long acquisition times. In this work we extended correlation MRS to an imaging modality and show that this can be realized *in-vivo* within feasible scan times. Combining optimized adiabatic excitation and spiral encoding we demonstrated the concept of correlation chemical shift imaging (CCSI). Two CCSI methods are introduced based on COSY and TOCSY, respectively. Although multivoxel COSY has been proposed previously (11–17), this work represents the first thorough demonstration of a robust and practical *in-vivo* CCSI which includes clinical applications of COSY based CCSI. Importantly, the TOCSY based CCSI is demonstrated for the first time.

Compared to COSY, TOCSY has the advantage of eliminating signal cancellation and improving spectral resolution with pure absorptive phase-sensitive crosspeaks obtained through coherent transfer of in-phase longitudinal magnetization (20). TOCSY provides also the entire set of correlations necessary for assignment, which could potentially help if ambiguities still exist in the COSY spectra. On the other hand, COSY spectra have a higher SNR than TOCSY because the optimum mixing conditions for TOCSY are harder to realize *in-vivo* within SAR limits. A TOCSY transfer efficiency of 50% has been obtained in single voxel in-vivo experiments at 3T for 64ms mixing with GOIA-W(16,4) pulses of 0.75 kHz amplitude (20). In addition, fully adiabatic TOCSY needs longer scanning times associated with longer repetition times. Hence, for *in-vivo* studies on human subjects presented in this work it was considered that COSY based CCSI represents a more feasible choice at 3T. Using COSY-LASER-SPIRAL sequence it was found that a matrix of 8×8 voxels (each 10 ml) can be recorded *in-vivo* at 3T with adequate SNR in 8:32 min. TOCSY-LASER-SPIRAL was demonstrated in healthy volunteers at 1.5T using similar matrix and voxels. 2D MRS at low magnetic fields could be useful to resolve larger metabolite overlap in 1D MRS due to reduced chemical shift dispersion. This can be relevant, since many clinical scanners operate in the range of 1.5T to 3T. In cases where SAR is less strict (phantoms, animal studies, other organs than brain) or when the acquisition time is not limited, TOCSY based CCSI may of course be a good option at 3T. An alternative at 3T, may be CCSI based on semi-adiabatic TOCSY (20), which would have a lower SAR and shorter repetition times. However PRESS or STEAM localization used in semi-adiabatic TOCSY will be affected by CSDE and will require optimized OVS (54,55) to reduce lipid contamination. Standard OVS saturation bands existing on clinical scanners do not provide adequate fat suppression for *in-vivo* CSI using PRESS or STEAM selection of VOI, as shown in Ref. (20). We intend to investigate this possibility in a future work.

A key step in the feasibility of this approach is constant-density spiral encoding which is highly time efficient. For an 8×8 matrix the minimum acquisition is 2s, becoming favorable

for dynamic spectroscopy. Further acceleration can be obtained with parallel spectroscopic imaging (56), and combining sparse k-space sampling with spiral encoding (28,57). Speed-up of 2D spectra acquisition can be also obtained by sparse sampling of t_1 dimension (58). For the same purpose, the method of ultra-fast single scan acquisition of multidimensional NMR spectra (59) could be adopted with suitable modification. Constant time evolution (31,60) could be employed in order to reduce the number of t_1 increments. The number of averages and of t_1 increments can be traded for more SNR, or for better resolution along f_1, depending on the limiting factor.

A minimum SNR of 10 was found *in-vivo* for COSY, while *in-vivo* TOCSY had a slightly lower minimum SNR of 8. The SNR could be increased with out-and-in spirals (61) or other self rewinding trajectories that can eliminate signal losses during the rewinder gradient. Optimal combination of MRS signal from multiple coils (62) by phase and baseline correcting the signal of each coil before their combination could increase sensitivity. Furthermore, SNR of 2D MRS can be improved if the signal of both crosspeaks is combined.

The 8×8 matrix (2×2 cm^2 in-plane spatial resolution) is sufficient in the human brain to separate regions with disease, such as tumors, from regions with healthier tissue. Point spread function simulations indicate that signal contamination due to ringing of the impulse function would not produce considerable signal contamination at this low resolution matrix. Voxel bleeding was not noticed in human subjects, though some voxel bleeding was observed in phantoms at high concentrations (lactate 50 mM, Fig. 3 in Supplementary Information). If necessary, application of a Hanning or Hamming window in the k-space can reduce ringing of point spread function, at the cost of altering in-plane voxel size. Extension to 3D spatial coverage of CCSI could be attempted by adding phase encoding along k_z direction as was shown for J-resolved spectra (30). A 3D matrix of 8×8×4 could be acquired in 8:32 min, if averaging is traded for phase encoding.

Adiabatic excitation with very large BW (20 kHz) pulses used in this work minimize chemical shift displacement error and provide optimal flip angles uniformly across large VOI and SW even in the presence of inhomogeneous RF fields. These features could be of interest also at high field (7T). The precise LASER localization provides artifact-free spectra. If optimal OVS (54,55) is available, a single spin-echo based slice selection that includes all the brain can be easily considered with GOIA-W(16,4) pulses. The low SAR of GOIA-W(16,4) enables repetition times that keep total scan time within feasible limits.

The *in-vivo* cases illustrate the potential of CCSI to resolve overlapped metabolites such as the total choline peak, GABA, glutamate, and threonine in normal subjects, or lactate and lipids in cancer. In disease CCSI could perhaps help to identify other important metabolites such as aspartate in the case of the tumor patient. Although aspartate and N-acetyl-aspartate are related metabolites they have different distribution in brain. While NAA is specific to neurons, aspartate can be synthesized both in astrocytes and neurons reversibly via transamination, and it can be transferred between the two cell types in both directions (63). Importantly, only astrocytes were shown to express the enzymes for de novo pyrimidine biosynthesis (64), and aspartate is one of the few substrates required for de novo pyrimidine synthesis. This could be relevant for tumors where nucleotides would be necessary for DNA during high mitotic activity of cancer cells. Since tumor cells in glioblastoma have an astrocytic origin it is likely that these tumors might contain increased levels of aspartate. This possibility is supported also by our previous work (4,53) with *ex-vivo* high quality 2D HRMAS that detects high aspartate in intact biopsies from glioblastoma patients. Although neuro-glial metabolism has been largely investigated in normal cell cells cultures or animals,

there are less data in the literature from *in-vivo* studies of human brain tumors related to aspartate. The significance of our findings remains to be investigated in more detail.

Compared to 1D spectral editing methods that filter out most of the metabolites in order to detect one metabolite of interest, 2D methods retain the full spectral information. In addition, the first t_1 increment of the CCSI experiments is available for analysis with the established methods (eg. LCModel, (65)) of conventional CSI. Nevertheless, more automated analysis (Profit, (66)) methods exist also for in-vivo 2D MRS.

Absolute quantification of *in-vivo* 2D MRS spectra could be done using ERETIC method (67), which would yield more precise results especially in disease than metabolite crosspeak to creatine diagonal peak volume ratio.

While these initial results are promising, *in-vivo* multi-spectral-spatial-dimensional MRS is a field that needs further development and validation. Advances in sequence design such as presented herein, reconstruction algorithms, and hardware development might improve the performance of 2D MRS through increased signal to noise ratio, better spatial resolution or shortened acquisition time. Future development could facilitate *in-vivo* biomedical applications of 2D MRS methods and further our knowledge of normal metabolism and disease.

Supplementary Material

Refer to Web version on PubMed Central for supplementary material.

Acknowledgments

References

1. Ernst RR. 2-Dimensional Spectroscopy. Chimia. 1975; 29(4):179–183.

2. Braunschweiler L, Ernst RR. Coherence Transfer by Isotropic Mixing - Application to Proton Correlation Spectroscopy. Journal of Magnetic Resonance. 1983; 53(3):521–528.

3. Pfeuffer J, Tkac I, Provencher SW, Gruetter R. Toward an in vivo neurochemical profile: Quantification of 18 metabolites in short-echo-time H-1 NMR spectra of the rat brain. Journal of Magnetic Resonance. 1999; 141(1):104–120. [PubMed: 10527748]

4. Andronesi OC, Mintzopoulos D, Struppe J, Black PM, Tzika AA. Solid-state NMR adiabatic TOBSY sequences provide enhanced sensitivity for multidimensional high-resolution magic-angle-spinning H-1 MR spectroscopy. Journal of Magnetic Resonance. 2008; 193(2):251–258. [PubMed: 18556227]

5. Griffin JL, Shockcor JP. Metabolic profiles of cancer cells. Nature Reviews Cancer. 2004; 4(7): 551–561.

6. Andronesi OC, Becker S, Seidel K, Heise H, Young HS, Baldus M. Determination of membrane protein structure and dynamics by magic-angle-spinning solid-state NMR spectroscopy. Journal of the American Chemical Society. 2005; 127(37):12965–12974. [PubMed: 16159291]

7. Griesinger C, Sorensen OW, Ernst RR. Two-Dimensional Correlation of Connected NMR Transitions. Journal of the American Chemical Society. 1985; 107(22):6394–6396.

8. Aue WP, Karhan J, Ernst RR. Homonuclear Broad-Band Decoupling and 2-Dimensional J-Resolved NMR-Spectroscopy. Journal of Chemical Physics. 1976; 64(10):4226–4227.

9. Thomas MA, Yue K, Binesh N, Davanzo P, Kumar A, Siegel B, Frye M, Curran J, Lufkin R, Martin P, Guze B. Localized two-dimensional shift correlated MR spectroscopy of human brain. Magnetic Resonance in Medicine. 2001; 46(1):58–67. [PubMed: 11443711]

10. Velan SS, Ramamurthy S, Ainala S, Durst C, Lemieux SK, Raylman RR, Spencer RG, Thomas MA. Implementation and validation of localized constant-time correlated spectroscopy (LCT-COSY) on a clinical 3T MRI scanner for investigation of muscle metabolism. J Magn Reson Imaging. 2007; 26(2):410–417. [PubMed: 17654733]

11. Ziegler A, Metzler A, Kockenberger W, Izquierdo M, Komor E, Haase A, Decorps M, VonKienlin M. Correlation-peak imaging. Journal of Magnetic Resonance Series B. 1996; 112(2):141–150. [PubMed: 8812898]

12. von Kienlin M, Ziegler A, Le Fur Y, Rubin C, Decorps M, Remy C. 2D-spatial/2D-spectral spectroscopic imaging of intracerebral gliomas in rat brain. Magnetic Resonance in Medicine. 2000; 43(2):211–219. [PubMed: 10680684]

13. Mayer D, Dreher W, Leibfritz D. Fast echo planar based correlation-peak imaging: Demonstration on the rat brain in vivo. Magnetic Resonance in Medicine. 2000; 44(1):23–28. [PubMed: 10893517]

14. Delmas F, Beloeil JC, van der Sanden BPJ, Nicolay K, Gillet B. Two-voxel localization sequence for in vivo two-dimensional homonuclear correlation spectroscopy. Journal of Magnetic Resonance. 2001; 149(1):119–125. [PubMed: 11273760]

15. Mayer D, Dreher W, Leibfritz D. Fast U-FLARE-based correlation-peak imaging with complete effective homonuclear decoupling. Magnetic Resonance in Medicine. 2003; 49(5):810–816. [PubMed: 12704762]

16. Verma, G.; Ramadan, S.; Lipnick, S.; Rajakumar, N.; Thomas, MA. Turbo Spin Echo Based Spatially Resolved Correlated Spectroscopic Imaging. Proceedings of the 16th ISMRM Scientific Meeting 2008; Toronto, Canada. p. 1602

17. Lipnick, S.; Ramadan, S.; Verma, G.; Thomas, MA. Echo-Planar based Correlated Spectroscopic Imaging (EP-COSI): Implementation and Evaluation in Human Skeletal Muscle Using a 3T MRI Scanner and a 8-channel Knee Coil. Proceedings of the 17th ISMRM Scientific Meeting 2009; Honolulu, Hawaii, USA. p. 4316

18. Choi IY, Lee SP, Shen J. Selective homonuclear Hartmann-Hahn transfer method for in vivo spectral editing in the human brain. Magnetic Resonance in Medicine. 2005; 53(3):503–510. [PubMed: 15723418]

19. Marjanska M, Henry PG, Bolan PJ, Vaughan B, Seaquist ER, Gruetter R, Ugurbil K, Garwood M. Uncovering hidden in vivo resonances using editing based on localized TOCSY. Magnetic Resonance in Medicine. 2005; 53(4):783–789. [PubMed: 15799065]

20. Andronesi OC, Ramadan S, Mountford CE, Sorensen AG. Low-power adiabatic sequences for in-vivo localized two-dimensional chemical shift correlated MR spectroscopy. Magnetic Resonance in Medicine. 2010; 64(6):1542–1556. [PubMed: 20890988]

21. Duyn JH, Moonen CTW. Fast Proton Spectroscopic Imaging of Human Brain Using Multiple Spin-Echoes. Magnetic Resonance in Medicine. 1993; 30(4):409–414. [PubMed: 8255188]

22. Dydak U, Meier D, Lamerichs R, Boesiger P. Trading spectral separation at 3T for acquisition speed in multi spin-echo spectroscopic imaging. Am J Neuroradiol. 2006; 27(7):1441–1446. [PubMed: 16908554]

23. Posse S, Tedeschi G, Risinger R, Ogg R, Lebihan D. High-Speed H-1 Spectroscopic Imaging in Human Brain by Echo-Planar Spatial-Spectral Encoding. Magnetic Resonance in Medicine. 1995; 33(1):34–40. [PubMed: 7891533]

24. Posse S, Decarli C, Lebihan D. 3-Dimensional Echo-Planar MR Spectroscopic Imaging at Short Echo Times in the Human Brain. Radiology. 1994; 192(3):733–738. [PubMed: 8058941]

25. Adalsteinsson E, Spielman DM. Spatially resolved two-dimensional spectroscopy. Magnetic Resonance in Medicine. 1999; 41(1):8–12. [PubMed: 10025605]

26. Adalsteinsson E, Irarrazabal P, Topp S, Meyer C, Macovski A, Spielman DM. Volumetric spectroscopic imaging with spiral-based k-space trajectories. Magnetic Resonance in Medicine. 1998; 39(6):889–898. [PubMed: 9621912]

27. Hiba B, Ziegler A. 2D J-resolved spiral spectroscopic imaging in rat brain at 7 T. Comptes Rendus Chimie. 2004; 7(3–4):201–206.

28. Mayer D, Kim DH, Spielman DM, Bammer R. Fast parallel spiral chemical shift imaging at 3T using iterative SENSE reconstruction. Magnetic Resonance in Medicine. 2008; 59(4):891–897. [PubMed: 18383298]

29. Kim DH, Margolis D, Xing L, Daniel B, Spielman D. In vivo prostate magnetic resonance spectroscopic imaging using two-dimensional J-resolved PRESS at 3 T. Magnetic Resonance in Medicine. 2005; 53(5):1177–1182. [PubMed: 15844143]

30. Kim DH, Henry R, Spielman DM. Fast multivoxel two-dimensional spectroscopic imaging at 3 T. Magnetic Resonance Imaging. 2007; 25(8):1155–1161. [PubMed: 17418519]

31. Mayer D, Kim DH, Adalsteinsson E, Spielman DM. Fast CT-PRESS-based spiral chemical shift imaging at 3 Tesla. Magnetic Resonance in Medicine. 2006; 55(5):974–978. [PubMed: 16586451]

32. Bottomley PA. Spatial Localization in NMR-Spectroscopy Invivo. Annals of the New York Academy of Sciences. 1987; 508:333–348. [PubMed: 3326459]

33. Frahm J, Bruhn H, Gyngell ML, Merboldt KD, Hanicke W, Sauter R. Localized High-Resolution Proton NMR-Spectroscopy Using Stimulated Echoes - Initial Applications to Human-Brain Invivo. Magnetic Resonance in Medicine. 1989; 9(1):79–93. [PubMed: 2540396]

34. Garwood M, DelaBarre L. The return of the frequency sweep: Designing adiabatic pulses for contemporary NMR. Journal of Magnetic Resonance. 2001; 153(2):155–177. [PubMed: 11740891]

35. Andronesi OC, Ramadan S, Ratai EM, Jennings D, Mountford CE, Sorensen AG. Spectroscopic imaging with improved gradient modulated constant adiabaticity pulses on high-field clinical scanners. Journal of Magnetic Resonance. 2010; 203(2):283–293. [PubMed: 20163975]

36. Mao J, Mareci TH, Andrew ER. Experimental-Study of Optimal Selective 180-Degrees Radiofrequency Pulses. Journal of Magnetic Resonance. 1988; 79(1):1–10.

37. Tannus A, Garwood M. Adiabatic pulses. NMR Biomed. 1997; 10(8):423–434. [PubMed: 9542739]

38. Levitt MH, Freeman R, Frenkiel T. Broad-Band Heteronuclear Decoupling. Journal of Magnetic Resonance. 1982; 47(2):328–330.

39. Andronesi OC, Ramadan S, Ratai EM, Mountford CE, Sorensen AG. Spectroscopic imaging with improved gradient modulated constant adiabaticity pulses on high-field clinical scanners. Journal of Magnetic Resonance. 2010; 203(2):283–293. [PubMed: 20163975]

40. Kupce E, Freeman R. Adiabatic Pulses for Wide-Band Inversion and Broad-Band Decoupling. Journal of Magnetic Resonance Series A. 1995; 115(2):273–276.

41. Ernst, RR.; Bodenhausen, G.; Wokaun, A. Principles of Nuclear Magnetic Resonance in One and Two Dimensions. Halpern, J.; Green, MLH.; Mukaiyama, T., editors. Oxford: Clarendon Press; 1987.

42. Haeberlen U, Waugh JS. Coherent Averaging Effects in Magnetic Resonance. Physical Review. 1968; 175(2) 453-&.

43. Levante TO, Baldus M, Meier BH, Ernst RR. Formalized Quantum-Mechanical Floquet Theory and Its Application to Sample-Spinning in Nuclear-Magnetic-Resonance. Molecular Physics. 1995; 86(5):1195–1212.

44. Smith SA, Levante TO, Meier BH, Ernst RR. Computer-Simulations in Magnetic-Resonance - an Object-Oriented Programming Approach. Journal of Magnetic Resonance Series A. 1994; 106(1): 75–105.

45. Govindaraju V, Young K, Maudsley AA. Proton NMR chemical shifts and coupling constants for brain metabolites. NMR Biomed. 2000; 13(3):129–153. [PubMed: 10861994]

46. Garwood M, Yong K. Symmetrical Pulses to Induce Arbitrary Flip Angles with Compensation for RF Inhomogeneity and Resonance Offsets. Journal of Magnetic Resonance. 1991; 94(3):511–525.

47. Kover KE, Uhrin D, Hruby VJ. Gradient- and sensitivity-enhanced TOCSY experiments. Journal of Magnetic Resonance. 1998; 130(2):162–168. [PubMed: 9500895]

48. Ogg RJ, Kingsley PB, Taylor JS. Wet, a T-1-Insensitive and B-1-Insensitive Water-Suppression Method for in-Vivo Localized H-1-NMR Spectroscopy. Journal of Magnetic Resonance Series B. 1994; 104(1):1–10. [PubMed: 8025810]

49. Glover GH. Simple analytic spiral K-space algorithm. Magnetic Resonance in Medicine. 1999; 42(2):412–415. [PubMed: 10440968]

50. van der Kouwe AJW, Benner T, Salat DH, Fischl B. Brain morphometry with multiecho MPRAGE. Neuroimage. 2008; 40(2):559–569. [PubMed: 18242102]

51. Beatty PJ, Nishimura DG, Pauly JM. Rapid gridding reconstruction with a minimal oversampling ratio. Ieee Transactions on Medical Imaging. 2005; 24(6):799–808. [PubMed: 15959939]

52. Lin YY, Hodgkinson P, Ernst M, Pines A. A novel detection-estimation scheme for noisy NMR signals: Applications to delayed acquisition data. Journal of Magnetic Resonance. 1997; 128(1): 30–41.

53. Andronesi OC, Blekas KD, Mintzopoulos D, Astrakas L, Black PM, Tzika AA. Molecular classification of brain tumor biopsies using solid-state magic angle spinning proton magnetic resonance spectroscopy and robust classifiers. International Journal of Oncology. 2008; 33(5): 1017–1025. [PubMed: 18949365]

54. Tran TKC, Vigneron DB, Sailasuta N, Tropp J, Le Roux P, Kurhanewicz J, Nelson S, Hurd R. Very selective suppression pulses for clinical MRSI studies of brain and prostate cancer. Magnetic Resonance in Medicine. 2000; 43(1):23–33. [PubMed: 10642728]

55. Martinez-Ramon M, Gallardo-Antolin A, Cid-Sueiro J, Heileman GL, Yung KT, Zheng WL, Zhao CG, Posse S. Automatic Placement of Outer Volume Suppression Slices in MR Spectroscopic Imaging of the Human Brain. Magnetic Resonance in Medicine. 2010; 63(3):592–600. [PubMed: 20187173]

56. Dydak U, Weiger M, Pruessmann KP, Meier D, Boesiger P. Sensitivity-encoded spectroscopic imaging. Magnetic Resonance in Medicine. 2001; 46(4):713–722. [PubMed: 11590648]

57. Gu M, Liu CL, Spielman DM. Parallel Spectroscopic Imaging Reconstruction with Arbitrary Trajectories Using k-Space Sparse Matrices. Magnetic Resonance in Medicine. 2009; 61(2):267–272. [PubMed: 19165883]

58. Freeman R, Kupce E. New ways to record multidimensional NMR spectra. Current Analytical Chemistry. 2006; 2(2):101–105.

59. Frydman L, Scherf T, Lupulescu A. The acquisition of multidimensional NMR spectra within a single scan. Proceedings of the National Academy of Sciences of the United States of America. 2002; 99(25):15858–15862. [PubMed: 12461169]

60. Dreher W, Leibfritz D. Detection of homonuclear decoupled in vivo proton NMR spectra using constant time chemical shift encoding: CT-PRESS. Magnetic Resonance Imaging. 1999; 17(1): 141–150. [PubMed: 9888407]

61. Hiba B, Faure B, Lamalle L, Decorps M, Ziegler A. Out-and-in spiral spectroscopic imaging in rat brain at 7 T. Magnetic Resonance in Medicine. 2003; 50(6):1127–1133. [PubMed: 14648560]

62. Prock T, Collins DJ, Dzik-Jurasz ASK, Leach MO. An algorithm for the optimum combination of data from arbitrary magnetic resonance phased array probes. Physics in Medicine and Biology. 2002; 47(2):N39–N46. [PubMed: 11841052]

63. Murín R, Mohammadi G, Kowtharapu B, Leibfritz D, Hamprecht B. Metabolism of [U-(13)C]aspartate by astroglial cultures: nuclear magnetic resonance analysis of the culture media. Neurochemical Research. 2010; 35(12):2053–2061. [PubMed: 21107687]

64. Cammer W, Downing M. Localization of the Multifunctional Protein Cad in Astrocytes of Rodent Brain. Journal of Histochemistry & Cytochemistry. 1991; 39(5):695–700. [PubMed: 1673139]

65. Provencher SW. Estimation of Metabolite Concentrations from Localized in-Vivo Proton NMR-Spectra. Magnetic Resonance in Medicine. 1993; 30(6):672–679. [PubMed: 8139448]

66. Schulte RF, Boesiger P. ProFit: two-dimensional prior-knowledge fitting of J-resolved spectra. NMR in Biomedicine. 2006; 19(2):255–263. [PubMed: 16541464]

67. Heinzer-Schweizer S, De Zanche N, Pavan M, Mens G, Sturzenegger U, Henning A, Boesiger P. In-vivo assessment of tissue metabolite levels using 1H MRS and the Electric REference To access In vivo Concentrations (ERETIC) method. NMR Biomed. 2010; 23(4):406–413. [PubMed: 20101606]

Abbreviation List

ADC **A**nalog to **D**igital **C**onverter

AHT	**A**verage **H**amiltonian **T**heory
Asp	**Asp**artate
BW	**B**and**w**idth
Cho	**Cho**line
CSI	**C**hemical **S**hift **I**maging
CCSI	**C**orrelation **C**hemical **S**hift **I**maging
COSY	**Co**rrelation **S**pectroscop**y**
CT-COSY	**C**onstant **T**ime **COSY**
CSDE	**C**hemichal **S**hift **D**isplacement **E**rror
EPI	**E**cho **P**lanar **I**maging
f$_1$, f$_2$	Indirect and direct detected **f**requency dimensions
FOV	**F**ield **O**f **V**iew
FWHM	**F**ull **W**idth at **H**alf **M**aximum
GABA	**G**amma-**a**mino-**b**utyric **a**cid
GBM	**G**lio**b**lasto**m**a
Glu	**Glu**tamate
GOIA	**G**radient **O**ffset **I**ndependent **A**diabaticity
GPC	**G**lycero-**p**hospho-**c**holine
HRMAS	**H**igh **R**esolution **M**agic **A**ngle **S**pinning
LASER	**L**ocalizer **A**diabatic **S**pin **E**cho **R**efocusing
Lac	**Lac**tate
L-COSY	**L**ocalized **COSY**
MLEV-16	**M**alcolm **Lev**itt's composite decoupling sequence
MRS	**M**agnetic **R**esonance **S**pectroscopy
Myo	**Myo**inositol
NA	**N**umber of **A**verages
NAA	**N**-**a**cetyl-**a**spartate
OVS	**O**uter **V**olume **S**uppresion
PC	**P**hospho-**c**holine
PE	**P**hospho-**e**thanolamine
PEPSI	**P**roton **E**cho **P**lanar **S**pectroscopic **I**maging
PRESS	**P**oint **R**esolved **S**pectroscopy
PSF	**P**oint **S**pread **F**unction
RF	**R**adio **F**requency
SAR	**S**pecific **A**bsorption **R**ate
SNR	**S**ignal to **N**oise **R**atio

STEAM	**S**timulated **E**cho **A**mplitude **M**odulated
SW	**S**pectral Band**w**idth
TE	**E**cho **T**ime
TR	**R**epetition **T**ime
t_{mix}, t_1, t_2	**mix**ing **t**ime, evolution **t**ime, detection **t**ime
TOCSY	**To**tal **C**orrelation **S**pectroscop**y**
Thr	**Thr**eonine
VOI	**V**olume **O**f **I**nterest
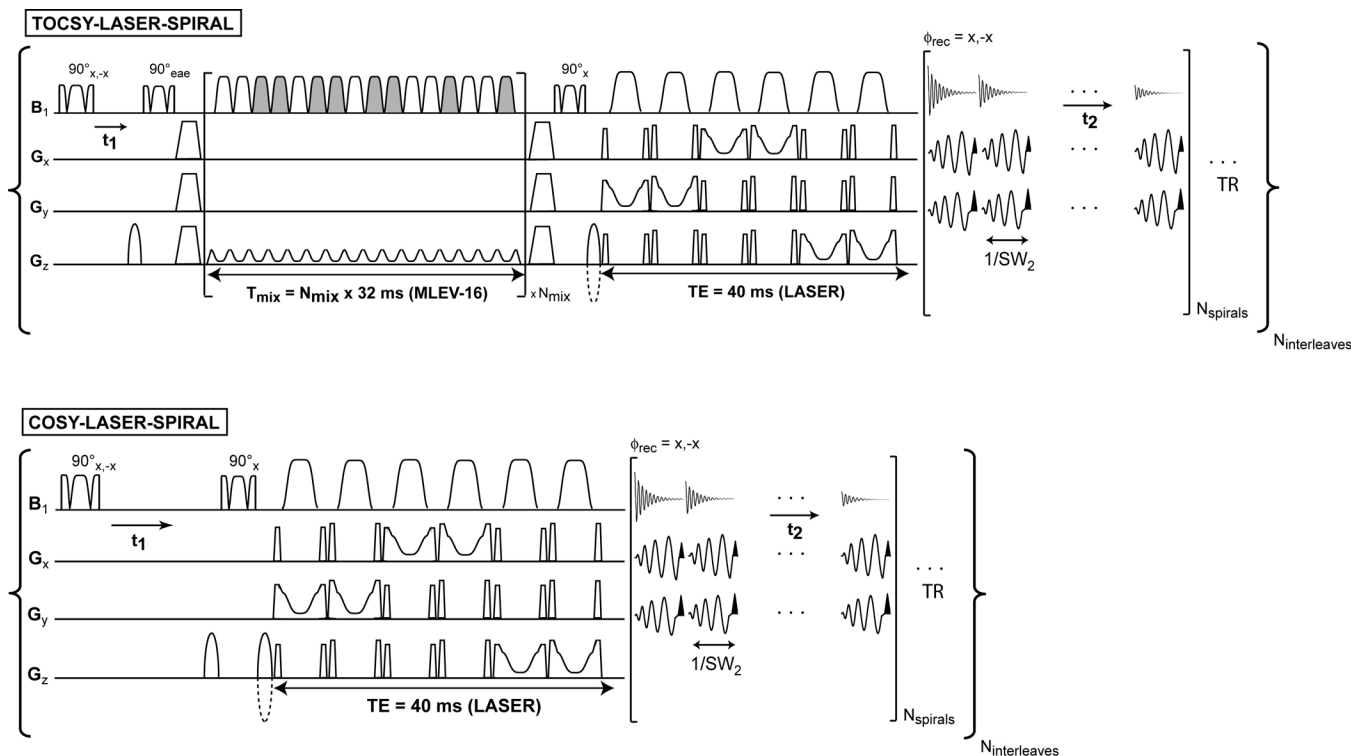
Figure 1.
CCSI pulse sequences for 2D-spectral/2D-spatial TOCSY-LASER-SPIRAL and COSY-LASER-SPIRAL experiments. LASER and GOIA-W(16,4) adiabatic pulses are used to select the desired VOI in both sequences (TE = 40ms). A gradient enhanced z-filter, composed of 90° adiabatic BIR-4 pulses and spoilers brackets the MLEV-16 block (pulses which are grayed-out have an overall 180° phase shift compared to non-grayed pulses, 64 ms total mixing time, $N_{mix} = 2$) to perform longitudinal mixing in TOCSY. Sine-bell shaped gradients select the coherence transfer pathway. Phase sensitive 2D spectra can be obtained with echo-antiecho acquisition if the polarity of gradients is alternated and the FID are stored separately, and for TOCSY the phase of the first 90° pulse of the z-filter is simultaneously alternated x to −x. The delay after the first 90° BIR-4 excitation pulse is incremented in consecutive experiments in order to encode the f_1 frequency dimension. The t_1 increment is inversely proportional to the desired spectral bandwidth in the f_1 frequency dimension. To eliminate the t_1 noise and improve water suppression in 2D spectra, a two step phase cycle is used, involving the first excitation pulse and the receiver. Spiral waveforms are played on the phase and readout gradients to acquire simultaneously two spatial dimensions and one frequency dimension (rewinding gradients for each spiral lobe are shown in black). The duration of a spiral lobe is inversely proportional to the desired spectral bandwidth (SW) in the f_2 frequency dimension. The spiral lobes are repeated ($N_{spirals} = 380$) within one acquisition window in order to encode the f_2 frequency dimension. The desired FOV, in-plane spatial resolution and SW are obtained by temporal and angular spiral interleaves ($N_{interleaves} = 2$ for 8×8 matrix, and $N_{interleaves} = 6$ for 16×16 matrix). The WET water suppression is not included in the pulse sequence diagrams. No OVS is necessary with LASER localization.
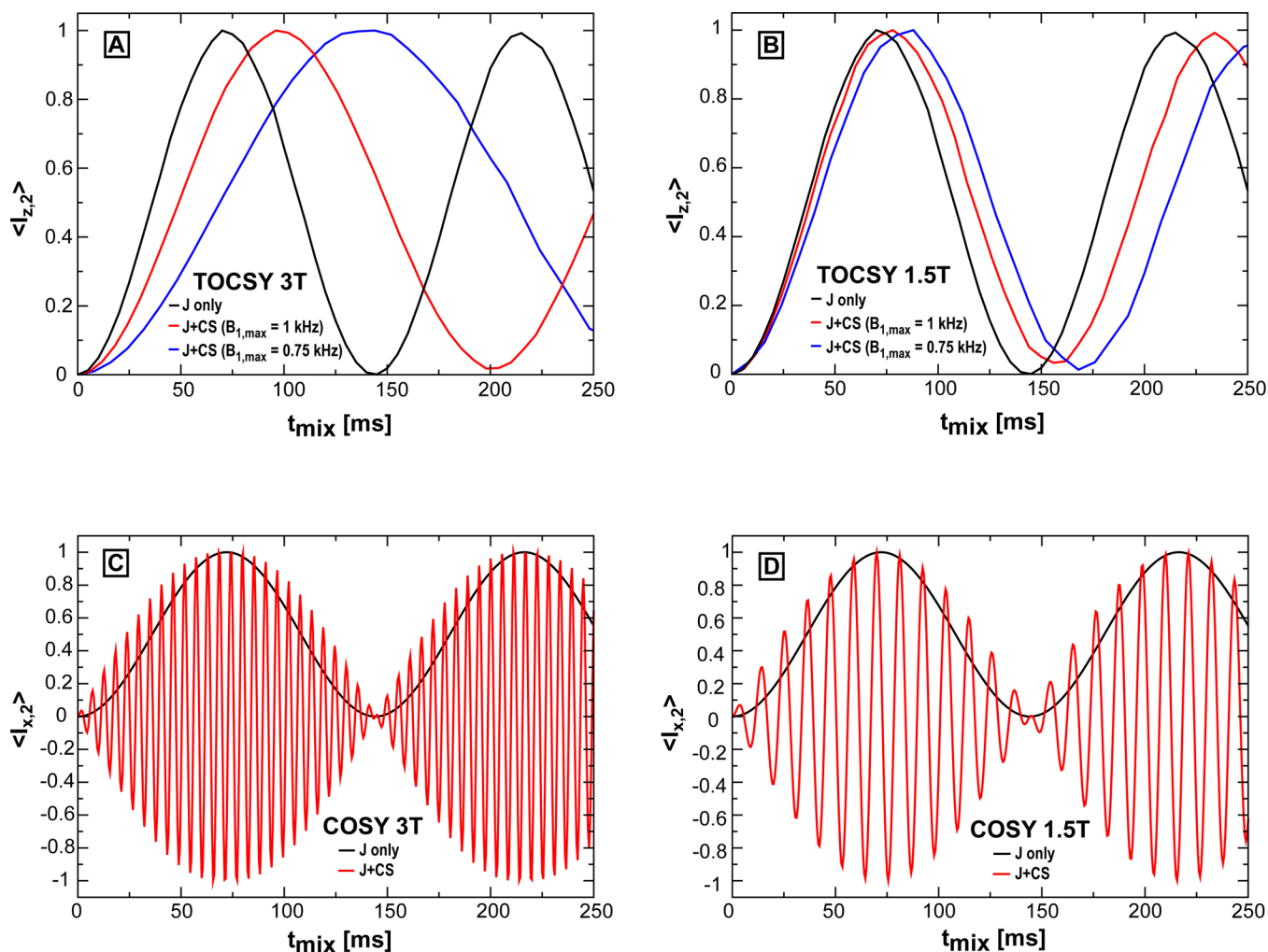
Figure 2.
Simulated buildup curves of crosspeaks for TOCSY and COSY at 3T and 1.5T in the case of a two spin system having the scalar coupling and chemical shifts of lactate. Ideal buildup curves obtained when only the scalar coupling is considered are shown in black. Longitudinal TOCSY mixing with MLEV-16 (Fig. 2A,B) is considered for two GOIA-W(16,4) pulses with a lower $B_{1,max}$ amplitude (0.75 kHz, blue line) and a higher $B_{1,max}$ amplitude (1 kHz, red line). Slower buildups are noticed for the lower $B_{1,max}$ field, corresponding to a weaker average Hamiltonian and a smaller effective scalar coupling. Transverse mixing for COSY results in rapid oscillations (red line, Fig. 2C,D) when chemical shifts are included, modulated by the slower scalar coupling buildup.
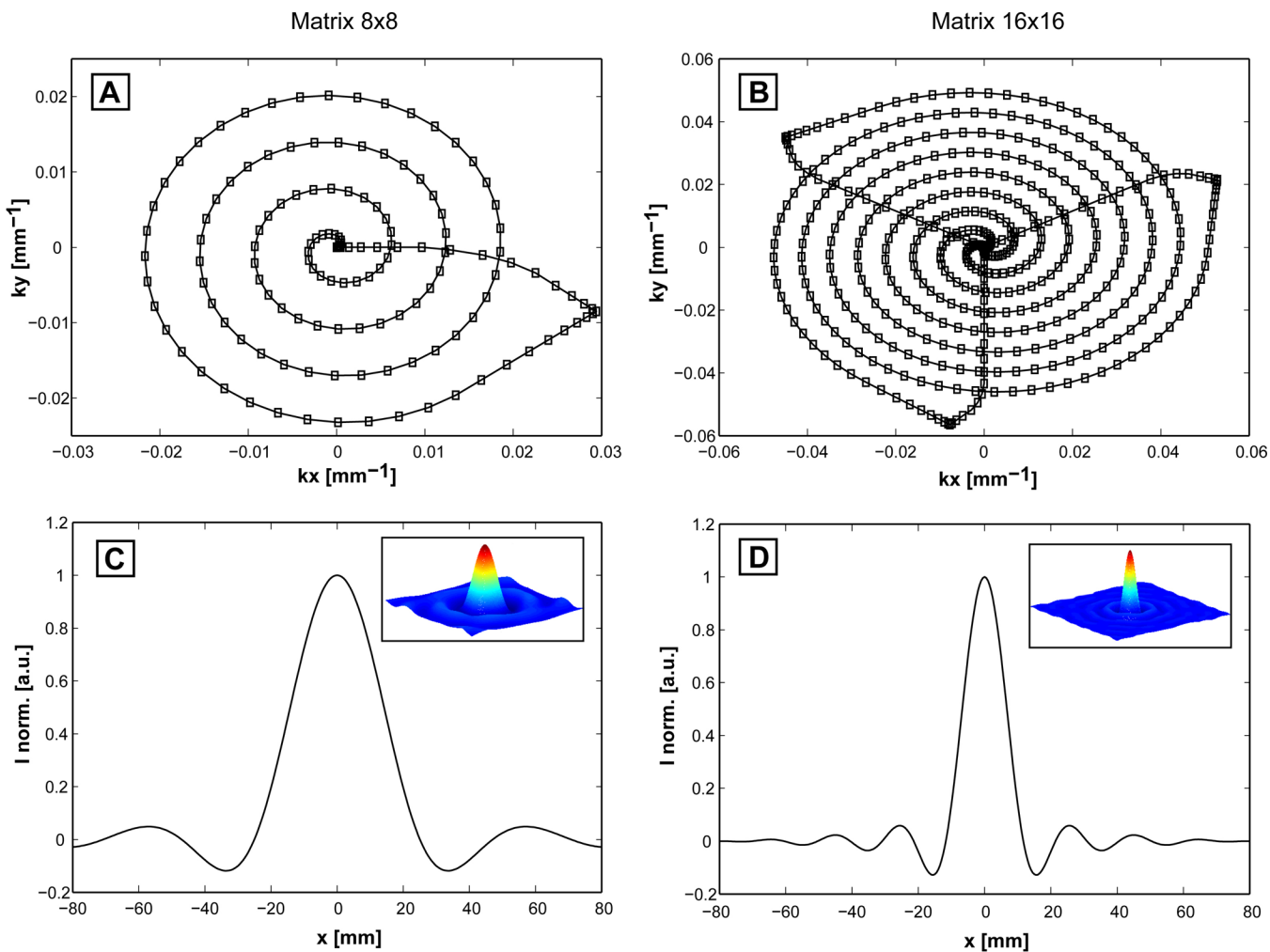
Matrix 8x8

Matrix 16x16

Figure 3.
Point spread function simulations for the 8×8 and 16×16 matrixes used for CCSI. The spiral trajectories designed to acquire the FOV = 16×16 cm^2 are shown for the 8×8 matrix (Fig. 3A, one angular interleave) and 16×16 matrix (Fig. 3B, three angular interleaves). Two temporal interleaves are necessary for SW = 1.2 kHz, obtained by delaying with 1/SW the angular interleaves in consecutive repetitions. PSF has a well defined main lobe with FWHM = 2 cm for 8×8 matrix, and FWHM = 1 cm for 16×16 matrix. The ringing of baseline does not indicate considerable voxel bleeding for any matrix, the ratio between the first positive sidelobe and the main lobe is 2.6% for 8×8 matrix, and 2.7% for 16×16 matrix.
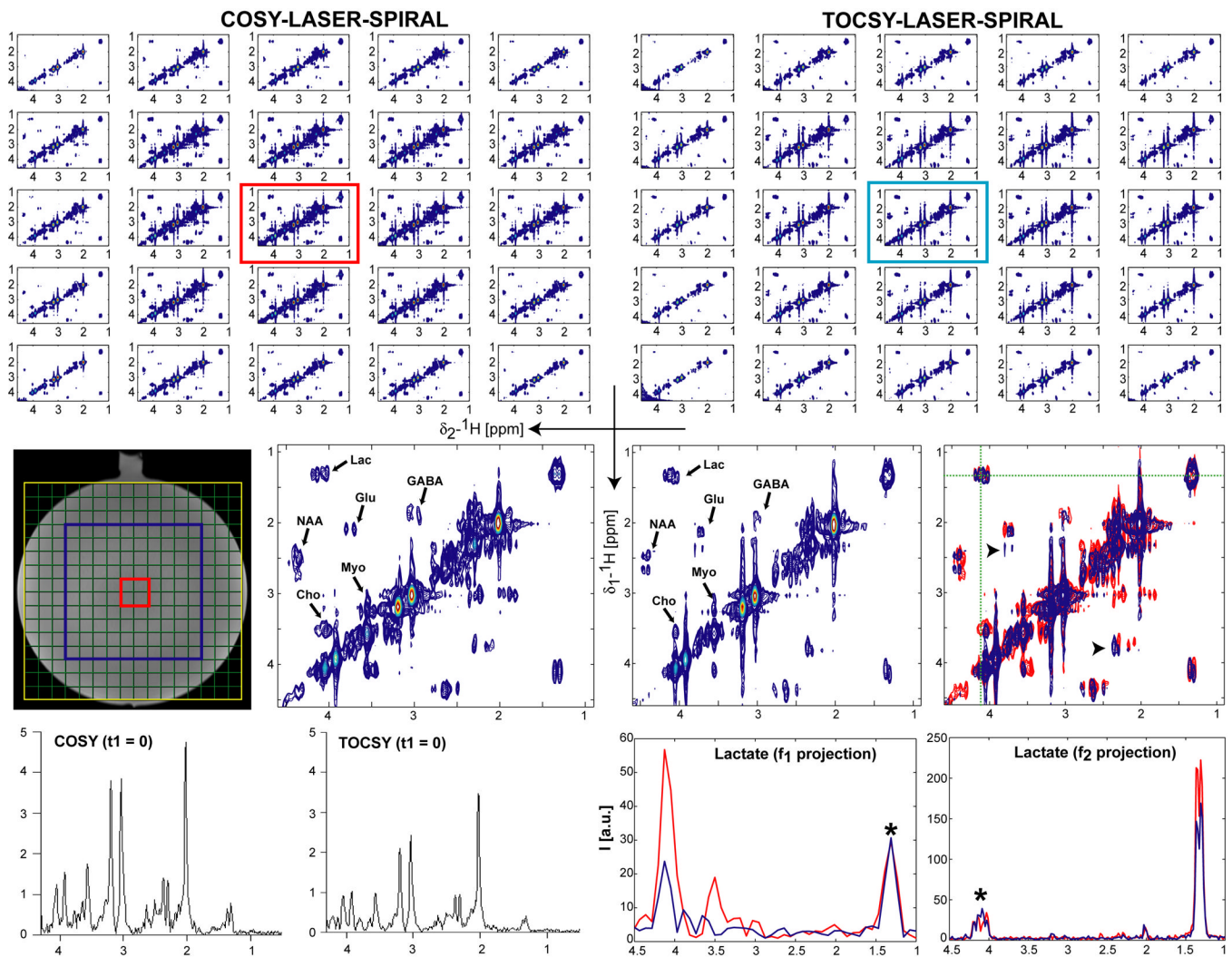
Figure 4.
CCSI at 3T in a homogeneous phantom containing brain metabolites at physiological concentrations. A large VOI (10×10 cm^2, slice thickness 2.5 cm, blue rectangle) is selected by LASER and imaged with spiral encoding (FOV = 16×16 cm^2 yellow rectangle, 8×8 acquisition matrix, $N_{interleaves}$ = 2, 2×2 cm^2 in-plane resolution, 10 ml voxel volume). Other acquisition parameters: 1) COSY – NA = 4, 64 t_1 increments, TR = 1s, 8:32 min acquisition time; 2) TOCSY – NA = 4, 64 t_1 increments, TR = 1.75s, 14:56 min acquisition time. The 1D spectral grids of each t_1 increment are interpolated to a 16×16 matrix (green grid) by the on-line ICE reconstruction program, however for 2D spectral analysis the spectra are reconstructed off-line on the acquired 8×8 matrix. Linear prediction to 128 points in t_1 using ITMPM method (Ref. (52)) and a shifted sine-squared window are applied in both t_1 and t_2 dimensions before FT. Crosspeaks can be assigned for all metabolites NAA, choline (Cho), glutamate (Glu), GABA, lactate (Lac), myoinositol (Myo). All the voxels within VOI, and an enlarged central voxel (red encircled) are shown. Note that narrower crosspeaks are obtained in the TOCSY spectra due to coherent transfer of in-phase longitudinal magnetization. An overlay between COSY (red) and TOCSY (blue) spectra from the central voxel is shown, the arrowheads indicate relay crosspeaks in TOCSY. Similar contour levels are displayed in COSY and TOCSY spectra. f_1 and f_2 projections through the lactate crosspeak show very good SNR (asterisk indicates the crosspeak, the other peak corresponds

to the diagonal peak). For COSY partial signal cancellation can be noticed as a notch in lactate crosspeak along f_2 projection, and slightly larger linewidths along both f_1 and f_2 projections (see also Fig. S4 in Supplementary Information). 1D spectra from the first t1 increment of COSY and TOCSY are shown for comparison.
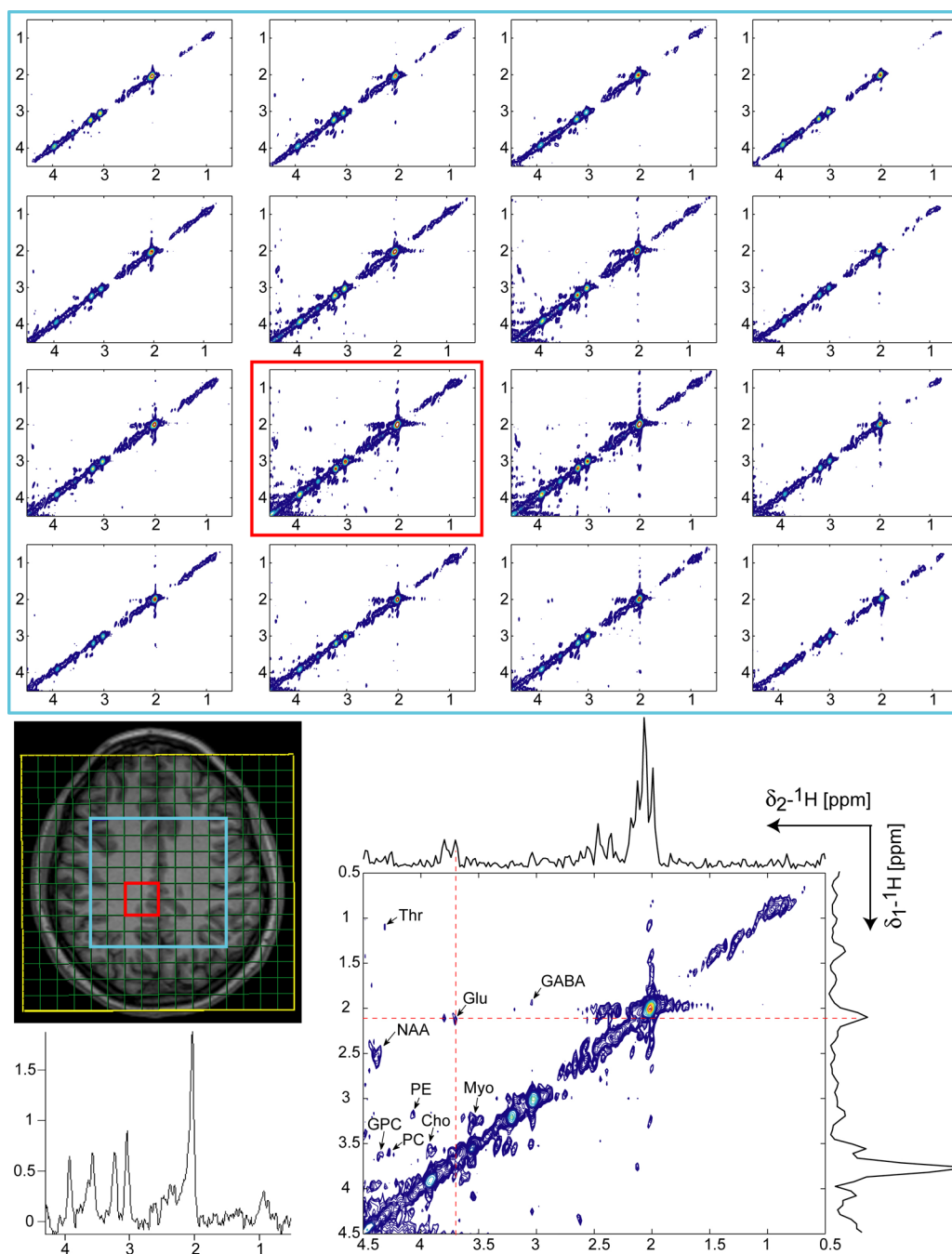
Figure 5.
CCSI acquired at 3T in 8:32 min using COSY-LASER-SPIRAL in a healthy volunteer. A VOI (8×8 cm^2, 2.5cm slice thickness, blue rectangle) is selected by LASER in centrum semiovale above the ventricles (no OVS was used around the skull). The same acquisition parameters and processing methods as in Fig. 4 were employed. The 4×4 voxels (each 10 ml) inside the VOI are shown together with an enlarged spectrum from a central voxel (red outlined). Crosspeaks of several metabolites can be clearly identified: NAA, Cho, Glu, GABA, Myo, GPC (Glycerophosphocholine), PC (Phosphocholine), PE (Phosphoethanolamine), and Threonine (Thr). In particular, resolving the total choline peak (Cho, GPC, PC) and GABA peak can be realized. f_1 and f_2 projections through the

glutamate crosspeak indicate the quality of 2D spectra (SNR and baseline). 1D spectrum from the first t1 increment is shown for comparison.
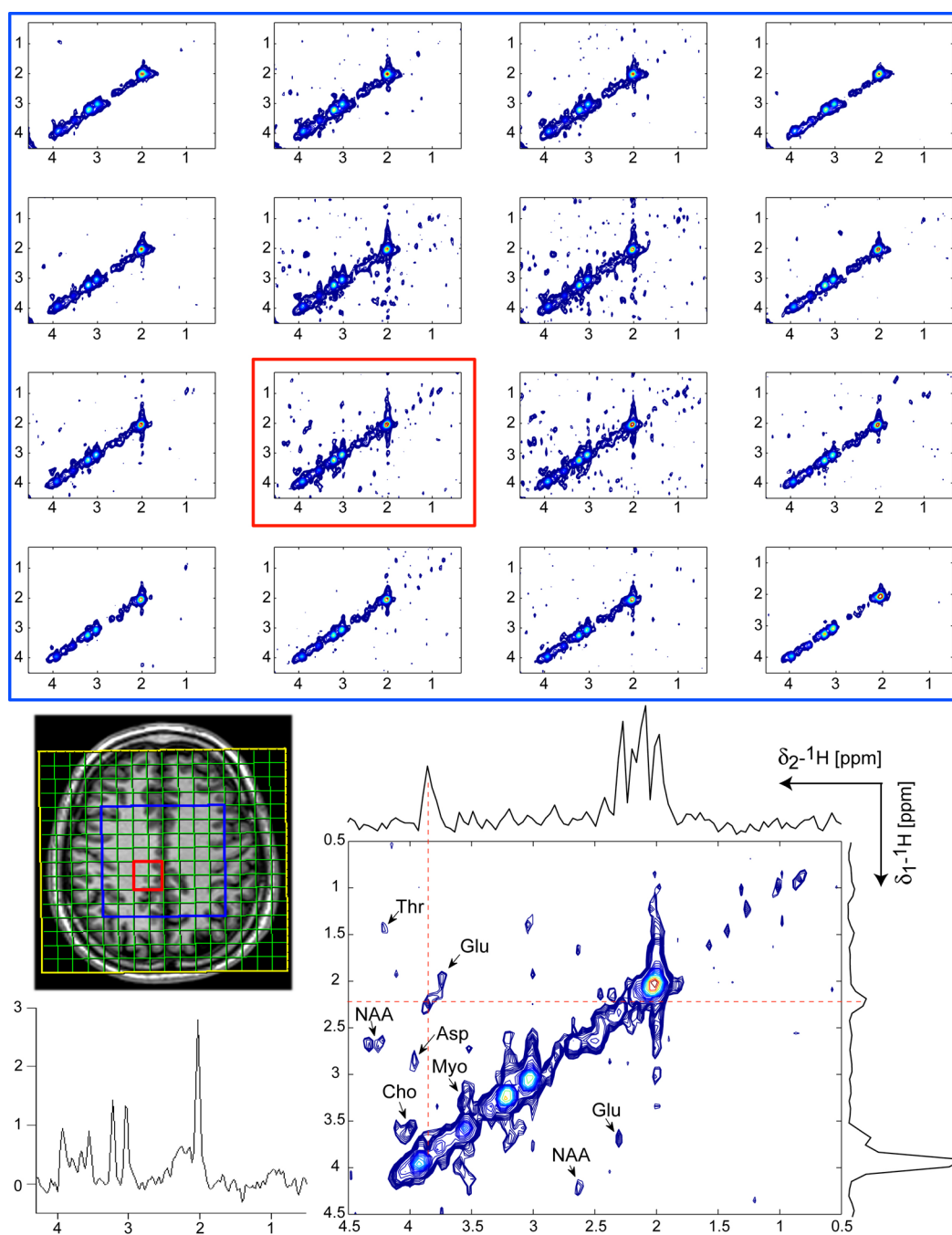
Figure 6.
CCSI acquired at 1.5T in 30 min using TOCSY-LASER-SPIRAL in a healthy volunteer. FOV of 16×16 cm^2, matrix 8×8, NA = 12, 50 t1 increments, TR = 1.5s and 32 ms TOCSY mixing time were used. A VOI (8×8 cm^2, 2.5cm slice thickness, blue rectangle) is selected by LASER in centrum semiovale above the ventricles (no OVS was used around the skull). The same processing methods like in Fig. 4 and 5 were employed. The 4×4 voxels (each 10 ml) inside the VOI are shown together with an enlarged spectrum from a central voxel (red outlined). Crosspeaks of several metabolites can be clearly identified: Aspartate (Asp), NAA, Cho, Glu, Myo, and Thr. Crosspeaks of GPC, PC, PE were not detected presumably due to shorter mixing time. f_1 and f_2 projections through the glutamate crosspeak indicate

the quality of 2D spectra (SNR and baseline). 1D spectrum from the first t1 increment is shown for comparison.
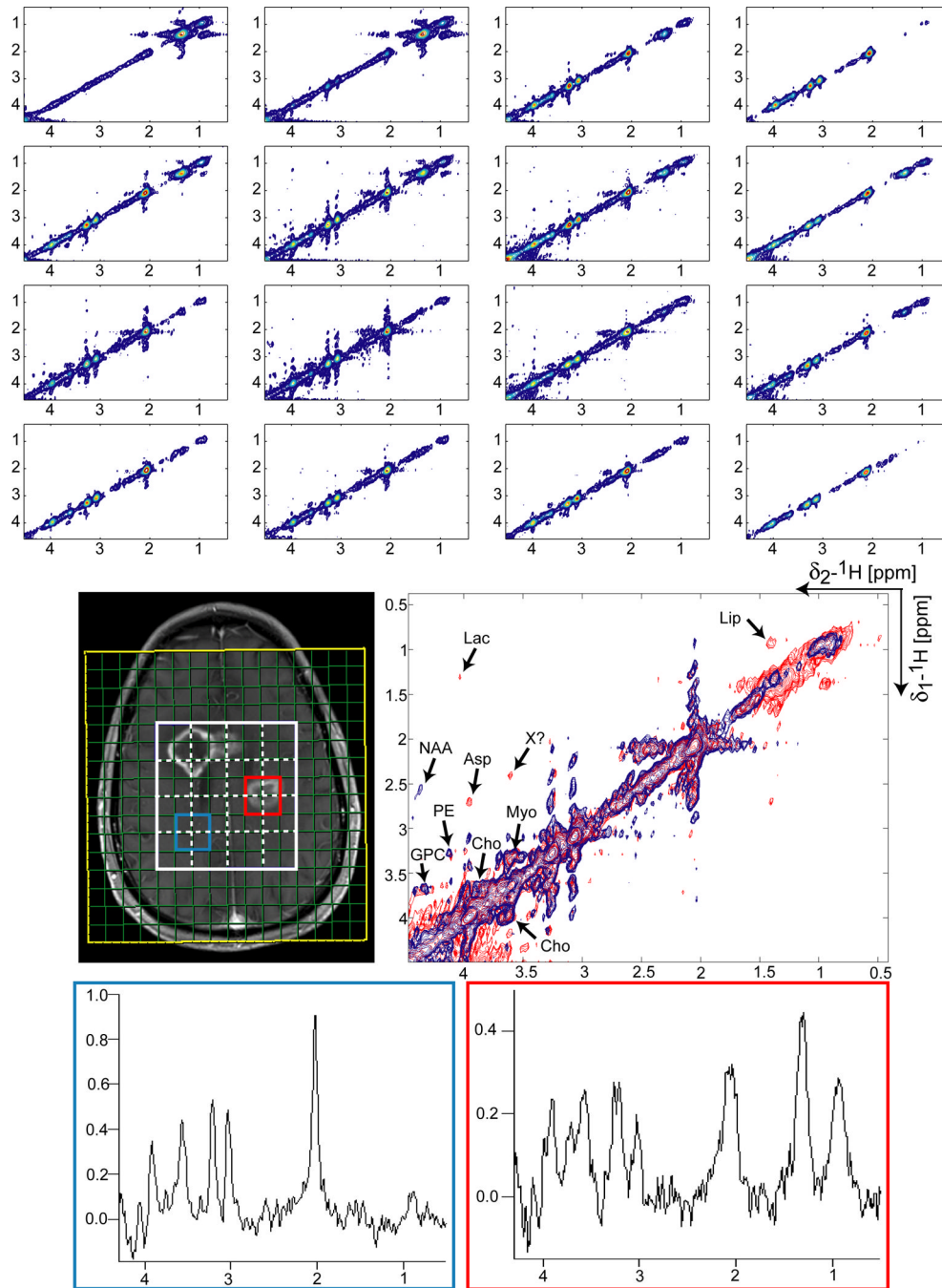
Figure 7.
CCSI acquired at 3T in 8:32 min using COSY-LASER-SPIRAL in a patient with a glioblastoma. A VOI (8×8 cm^2, 2.5cm slice thickness, white rectangle) is selected by LASER on the post contrast MEMPRAGE image to include both tumor foci (no OVS was used around the skull). The same acquisition parameters and processing methods as in Figs. 4 and 5 were employed. All the 4×4 voxels (each 10 ml) inside the VOI are shown. The dashed white lines on the MEMPRAGE image indicate the grid of the 4×4 voxels. It can be noticed that the 2×2 cm^2 in-plane spatial resolution of the 2D spectra can discriminate the tumor distribution. An overlay between a tumor spectrum (sum of voxels outlined by red line) and a spectrum from a healthier region (sum of voxels outlined by blue line) is shown.

In the tumor spectrum lactate (Lac) and lipid (Lip) signals are clearly separated. By comparison in the 1D spectra originating from the same voxels shown bellow, the lactate and lipid overlap completely. Choline, GPC and PE do not seem to be enhanced in the tumor, as indicated also by the total choline peak of the 1D spectra. Aspartate (Asp) signal is detected in tumor which can be biologically relevant for tumor metabolism. A distinct crosspeak X seems to be present at 3.6/2.3 ppm (f_2/f_1) in the tumor spectrum which could match the Hα-Hβ correlation of valine, although this assignment can be made only tentatively.

Table 1

Signal to noise ratio (SNR) of COSY and TOCSY experiments. The SNR of crosspeaks (SNR_c) and of diagonal peaks (SNR_d) is calculated as the maximum signal intensity over the standard deviation of noise. The noise level was estimated in a signal free region of the 2D spectrum (0.5ppm-0ppm / 0.5ppm-0ppm). The maximum signal intensity was considered for the crosspeaks located at $(f_2/f_1)_c$ and for diagonal peaks located at $(f_2/f_1)_d$ in the 2D spectra (ppm scale). Only one of the crosspeaks was considered, however the signal of both crosspeaks can be combined to increase the SNR of 2D MRS.

Phantoms — COSY

	NAA	Cho	Glu	Lac	Myo	NAA
SNR_c	49.5[a]	50.3[a]	29.5	37.4	83.5	21.1
SNR_d	1931.6	1639.2	220.7	244.4	321.6	654.3
$(f_2/f_1)_c$	4.38/2.67	4.05/3.5	3.74/2.12	4.09/1.31	3.61/3.26	4.38/2.67
$(f_2/f_1)_d$	2.01/2.01	3.19/3.19	2.33/2.33	1.31/1.31	3.61/3.61	2.01/2.01

Phantoms — TOCSY

	NAA	Cho	Glu	Lac	Myo	Asp
SNR_c	25.9[a]	33.1[a]	22.7	38.3	39.2	8.9
SNR_d	1838.0	649.8	141.2	165.7	184.8	15.7
$(f_2/f_1)_c$	4.38/2.67	4.05/3.5	3.74/2.12	4.09/1.31	3.61/3.26	3.89/2.8
$(f_2/f_1)_d$	2.01/2.01	3.19/3.19	2.33/2.33	1.31/1.31	3.61/3.61	2.8/2.8

Volunteers — COSY

	Cho	GPC	PC	PE	Glu	Myo	Thr
SNR_c	14.2	12.2	14.0	12.8	12.1	25.3	10.3
SNR_d		354.1[b]			73.5	136.6	15.8
$(f_2/f_1)_c$	4.05/3.5	4.31/3.66	4.28/3.64	3.97/3.21	3.74/2.12	3.61/3.26	4.24/1.32
$(f_2/f_1)_d$		3.2/3.2[b]			2.33/2.33	3.61/3.61	1.32/1.32

Volunteers — TOCSY

	NAA	Cho	Glu	Myo	Thr
SNR_c	10.8[a]	14.7[a]	11.6	14.8	8.0
SNR_d	804.2	459.5[b]	38.3	163.6	11.1
$(f_2/f_1)_c$	4.38/2.67	4.05/3.5	3.74/2.12	3.61/3.26	4.24/1.32
$(f_2/f_1)_d$	2.01/2.01	3.2/3.2[b]	2.33/2.33	3.61/3.61	1.32/1.32

[a] the small ratio between crosspeaks and diagonal peaks volumes noticed for NAA and Cho is due to the fact that considerable more protons contribute for the diagonal peaks (3 for NAA, 9 for Cho) compared to crosspeaks (1 for NAA, 2 for Cho);

[b] the total Choline peak (3.2 ppm) was considered as diagonal peak in the case of volunteers for Cho, GPC, PC and PE.

Table 2

Volumes of the crosspeaks (Vc) and diagonal peaks (Vd) in COSY and TOCSY experiments. The volumes of crosspeaks and diagonal peaks were integrated for the peaks centered at the same positions mentioned in Table 1 (Cre diagonal peak was considered at 3.02/3.02 ppm). The ratio of crosspeaks to diagonal peaks volumes (Vc/Vd) is calculated in each case, and is indicative of transfer efficiency. The ratio of TOCSY to COSY crosspeak volumes (Vc^t/Vc^e) was estimated in the case of phantom experiments that were done on the same 3T scanner and phantom. For volunteer this was not attempted since different scanners (3T for COSY and 1.5T for TOCSY) and different volunteers were used.

Phantoms

COSY

	NAA	Cho	Glu	Lac	Myo	Cre
Vc	1172	885	691	810	592	
Vd	10803	9162	1941	3156	2382	9355
Vc/Vd	0.11^a	0.10^a	0.36	0.26	0.25	

TOCSY

	NAA	Cho	Glu	Lac	Myo	Cre
Vc	818	420	708	792	336	
Vd	10380	8107	886	2551	1565	7269
Vc/Vd	0.08^a	0.05^a	0.80	0.31	0.22	
Vc^t/Vc^e	0.53	0.66	0.77	1.02	0.47	

Volunteers

COSY

	NAA	Cho	GPC	PC	PE	Glu	Myo	Thr	Cre
Vc	377	208	127	75	91	280	540	62	
Vd	4820		2405^b			581	878	164	2405
Vc/Vd	0.08^a	0.09^a	0.05	0.03	0.04	0.48	0.62	0.38	

TOCSY

	Asp	NAA	Cho	Glu	Myo	Thr	Cre
Vc	372	649	618	1170	775	266	
Vd	903	15818	11252^b	3235	5611	1387	5048
Vc/Vd	0.41	0.04^a	0.05^a	0.36	0.14	0.19	

a) the small ratio between crosspeaks and diagonal peaks volumes noticed for NAA and Cho is due to the fact that considerable more protons contribute for the diagonal peaks (3 for NAA, 9 for Cho) compared to crosspeaks (1 for NAA, 2 for Cho);

b) the total Choline peak (3.2 ppm) was considered as diagonal peak in the case of volunteers for Cho, GPC, PC and PE.